[4] Y. Ichijima, K. Yoshioka, Y. Yoshioka, K. Shinohe, H. Fujimori, J. Unno, M. Takagi, H. Goto, M. Inagaki, S. Mizutani, H. Teraoka, DNA lesions induced by replication stress trigger mitotic aberration and tetraploidy development, PloS One 5 (2010) e8821.
[5] A. Matheu, A. Maraver, P. Klatt, I. Flores, I. Garcia-Cao, C. Borras, J.M. Flores, J. Vina, M.A. Blasco, M. Serrano, Delayed ageing through damage protection by the Arf/p53 pathway, Nature 448 (2007) 375–379.
[6] K. Yoshioka, Y. Atsumi, H. Fukuda, M. Masutani, H. Teraoka, The quiescent cellular state is Arf/p53-dependent and associated with H2AX downregulation and genome stability, International Journal of Molecular Sciences 13 (2012) 6492–6506.
[7] Y. Atsumi, H. Fujimori, H. Fukuda, A. Inase, K. Shinohe, Y. Yoshioka, M. Shikanai, Y. Ichijima, J. Unno, S. Mizutani, N. Tsuchiya, Y. Hippo, H. Nakagama, M. Masutani, H. Teraoka, K. Yoshioka, Onset of quiescence following p53 mediated down-regulation of H2AX in normal cells, PloS One 6 (2011) e23432.
[8] C.A. Brady, D. Jiang, S.S. Mello, T.M. Johnson, L.A. Jarvis, M.M. Kozak, D. Kenzelmann Broz, S. Basak, E.J. Park, M.E. McLaughlin, A.N. Karnezis, L.D. Attardi, Distinct p53 transcriptional programs dictate acute DNA-damage responses and tumor suppression, Cell 145 (2011) 571–583.
[9] T. Li, N. Kon, L. Jiang, M. Tan, T. Ludwig, Y. Zhao, R. Baer, W. Gu, Tumor suppression in the absence of p53-mediated cell-cycle arrest, apoptosis, and senescence, Cell 149 (2012) 1269–1283.
[10] L.A. Donehower, M. Harvey, B.L. Slagle, M.J. McArthur, C.A. Montgomery Jr., J.S. Butel, A. Bradley, Mice deficient for p53 are developmentally normal but susceptible to spontaneous tumours, Nature 356 (1992) 215–221.
[11] T. Kamijo, F. Zindy, M.F. Roussel, D.E. Quelle, J.R. Downing, R.A. Ashmun, G. Grosveld, C.J. Sherr, Tumor suppression at the mouse INK4a locus mediated by the alternative reading frame product p19ARF, Cell 91 (1997) 649–659.
[12] D.A. Liebermann, B. Hoffman, D. Vesely, P53 induced growth arrest versus apoptosis and its modulation by survival cytokines, Cell Cycle 6 (2007) 166–170.
[13] C. Lu, W.S. El-Deiry, Targeting p53 for enhanced radio- and chemo-sensitivity, Apoptosis: An International Journal on Programmed Cell Death 14 (2009) 597–606.
[14] H.F. Ding, D.E. Fisher, Mechanisms of p53-mediated apoptosis, Critical Reviews in Oncogenesis 9 (1998) 83–98.
[15] S.D. Tyner, S. Venkatachalam, J. Choi, S. Jones, N. Ghebranious, H. Igelmann, X. Lu, G. Soron, B. Cooper, C. Brayton, S.H. Park, T. Thompson, G. Karsenty, A. Bradley, L.A. Donehower, P53 mutant mice that display early ageing-associated phenotypes, Nature 415 (2002) 45–53.
[16] B. Maier, W. Gluba, B. Bernier, T. Turner, K. Mohammad, T. Guise, A. Sutherland, M. Thorner, H. Scrable, Modulation of mammalian life span by the short isoform of p53, Genes & Development 18 (2004) 306–319.
[17] G.W. Hinkal, C.E. Gatza, N. Parikh, L.A. Donehower, Altered senescence, apoptosis, and DNA damage response in a mutant p53 model of accelerated aging, Mechanisms of Ageing and Development 130 (2009) 262–271.
[18] O.A. Sedelnikova, I. Horikawa, D.B. Zimonjic, N.C. Popescu, W.M. Bonner, J.C. Barrett, Senescing human cells and ageing mice accumulate DNA lesions with unrepairable double-strand breaks, Nature Cell Biology 6 (2004) 168–170.
[19] W.M. Bonner, C.E. Redon, J.S. Dickey, A.J. Nakamura, O.A. Sedelnikova, S. Solier, Y. Pommier, GammaH2AX and cancer, Nature Reviews Cancer 8 (2008) 957–967.
[20] C.H. Bassing, F.W. Alt, H2AX may function as an anchor to hold broken chromosomal DNA ends in close proximity, Cell Cycle 3 (2004) 149–153.
[21] D.R. Pilch, O.A. Sedelnikova, C. Redon, A. Celeste, A. Nussenzweig, W.M. Bonner, Characteristics of gamma-H2AX foci at DNA double-strand breaks sites, Biochemistry and Cell Biology 81 (2003) 123–129.
[22] O. Fernandez-Capetillo, A. Lee, M. Nussenzweig, A. Nussenzweig, H2AX: the histone guardian of the genome, DNA Repair 3 (2004) 959–967.
[23] K. Yoshioka, Y. Yoshioka, P. Hsieh, ATR kinase activation mediated by MutSalpha and MutLalpha in response to cytotoxic O6-methylguanine adducts, Molecular Cell 22 (2006) 501–510.
[24] G.J. Todaro, H. Green, Quantitative studies of the growth of mouse embryo cells in culture and their development into established lines, The Journal of Cell Biology 17 (1963) 299–313.
[25] S.W. Lowe, T. Jacks, D.E. Housman, H.E. Ruley, Abrogation of oncogene-associated apoptosis allows transformation of p53-deficient cells, Proceedings of the National Academy of Sciences of the United States of America 91 (1994) 2026–2030.
[26] I.H. Lee, Y. Kawai, M.M. Fergusson, I.I. Rovira, A.J. Bishop, N. Motoyama, L. Cao, T. Finkel, Atg7 modulates p53 activity to regulate cell cycle and survival during metabolic stress, Science 336 (2012) 225–228.
[27] T.A. Chan, H. Hermeking, C. Lengauer, K.W. Kinzler, B. Vogelstein, 14-3-3Sigma is required to prevent mitotic catastrophe after DNA damage, Nature 401 (1999) 616–620.
[28] I. Vitale, L. Galluzzi, M. Castedo, G. Kroemer, Mitotic catastrophe: a mechanism for avoiding genomic instability, Nature Reviews Molecular Cell Biology 12 (2011) 385–392.
[29] M. Zajac, M.V. Moneo, A. Carnero, J. Benitez, B. Martinez-Delgado, Mitotic catastrophe cell death induced by heat shock protein 90 inhibitor in BRCA1-deficient breast cancer cell lines, Molecular Cancer Therapeutics 7 (2008) 2358–2366.
[30] J.B. Stevens, G. Liu, S.W. Bremer, K.J. Ye, W. Xu, J. Xu, Y. Sun, G.S. Wu, S. Savasan, S.A. Krawetz, C.J. Ye, H.H. Heng, Mitotic cell death by chromosome fragmentation, Cancer Research 67 (2007) 7686–7694.
[31] J. Portugal, S. Mansilla, M. Bataller, Mechanisms of drug-induced mitotic catastrophe in cancer cells, Current Pharmaceutical Design 16 (2010) 69–78.
[32] H. Fujimori, M. Shikanai, H. Teraoka, M. Masutani, K. Yoshioka, Induction of cancerous stem cells during embryonic stem cell differentiation, The Journal of Biological Chemistry 287 (2012) 36777–36791.

Biochemical and Biophysical Research Communications 434 (2013) 15–21

Contents lists available at SciVerse ScienceDirect

Biochemical and Biophysical Research Communications

journal homepage: www.elsevier.com/locate/ybbrc

Poly(ADP-ribosylation) regulates chromatin organization through histone H3 modification and DNA methylation of the first cell cycle of mouse embryos

Tomoharu Osada [a,b,*], Anna-Margareta Rydén [c], Mitsuko Masutani [c,*]

[a] Advanced Medical Science Research Department, Mitsubishi Chemical Medience Corporation, 14-1 Sunayama, Kamisu-shi, Ibaragi 314-0255, Japan
[b] Department of Regenerative and Developmental Biology, Mitsubishi Kagaku Institute of Life Sciences (MITILS), 11 Minamiooya, Machida-shi, Tokyo 194-8511, Japan
[c] Division of Genome Stability Research, National Cancer Center Research Institute, 5-1-1 Tsukiji, Chuo-ku, Tokyo 104-0045, Japan

ARTICLE INFO

Article history:
Received 3 March 2013
Available online 30 March 2013

Keywords:
Fertilization
Histone modification
DNA methylation
Poly(ADP-ribosylation)
Post-translational modification

ABSTRACT

We examined the roles of poly(ADP-ribosylation) in chromatin remodeling during the first cell cycle of mouse embryos. Drug-based inhibition of poly(ADP-ribosylation) by a PARP inhibitor, PJ-34, revealed up-regulation of dimethylation of histone H3 at lysine 4 in male pronuclei and down-regulation of dimethylation of histone H3 at lysine 9 (H3K9) and lysine 27 (H3K27). Association of poly(ADP-ribosylation) with histone modification was suggested to be supported by the interaction of Suz12, a histone methyltransferase in the polycomb complex, with Parp1. PARP activity was suggested to be required for a proper localization and maintenance of Suz12 on chromosomes. Notably, DNA methylation level of female pronuclei in one-cell embryos was robustly decreased by PJ-34. Electron microscopic analysis showed a frequent appearance of unusual electron-dense areas within the female pronuclei, implying the disorganized and hypercondensed chromatin ultrastructure. These results show that poly(ADP-ribosylation) is important for the integrity of non-equivalent epigenetic dynamics of pronuclei during the first cell cycle of mouse embryos.

1. Introduction

Poly(ADP-ribosylation) (PARylation) is an instant posttranslational modification of protein and is involved in many cellular processes [1,2]. In particular, recent studies have revealed its essential roles in chromatin remodeling for transcription [3–6]. Modification of PARylation triggers loosening of chromatin structure, which enables the access of transcriptional factors to the DNA duplex structure. In addition, poly(ADP-ribose) polymerase (PARP) is localized mainly on chromatin of transcriptionally active genes, which are clearly segregated from the localization of histone H1 on transcriptionally-suppressed genes [7]. However, it is not clear how PARylation affects transcription-independent chromatin remodeling of the first cell cycle of mouse development.

During the first cell cycle of mouse embryos, a few genes are transcribed mainly from paternal genome [8,9]. Inhibition of transcription during one-cell embryos by RNA polymerase inhibitors showed the dispensable roles of RNA polymerases at the beginning of mouse development [10]. However, zygotic gene activation is required for progression from 2-cell to 4-cell embryos [11,12]. These findings indicate that posttranslational regulation of protein should act as a stem mechanism of the development of one-cell embryos. Upon fertilization, highly compacted chromatin of gametes was acutely decondensed to form pronuclei within a few hours. Protamines of sperm chromatin are replaced by maternal histone H1 during this process, which may be associated with global DNA hypomethylation of sperm-derived pronuclei (PN) [13,14]. In contrast, maternal chromatin arrested at metaphase II progressed rapidly into G1 phase and subsequently forms the female PN. DNA synthesis from paternal genome is preceded to that from maternal DNA. A minor transcription is activated solely from male pronuclei. This evidence suggests that the requirement for the posttranslational regulations of parental genomes before mingling of both gamete DNA to begin the proper zygotic development.

Of posttranslational modification of proteins, we examined here the effects of PARylation during the first cell cycle of mouse embryos, because metabolism of NAD, which is the substrate of PARPs, is acutely activated upon fertilization [15,16]. We previously showed that PARP inhibitor blocked pronuclear fusion at pronuclear envelop breakdown, with defective polymerization of tubulins, reduced MAPK signaling, and decreased phosphorylation of lamin A/C [17,18]. However, the role of PARylation in chromatin regulation in one-cell embryos is yet to be elucidated. Here we further studied the functions of PARylation in non-equivalent

* Corresponding authors. Address: Advanced Medical Science Research Department, Mitsubishi Chemical Medience Corporation, 14-1 Sunayama, Kamisu-shi, Ibaragi 314-0255, Japan (T. Osada). Division of Genome Stability Research, National Cancer Center Research Institute, 5-1-1 Tsukiji, Chuo-ku, Tokyo 104-0045, Japan (M. Masutani).

E-mail addresses: osada.tomoharu@mg.medience.co.jp (T. Osada), mmasutan@ncc.go.jp (M. Masutani).

0006-291X/$ - see front matter © 2013 Elsevier Inc. All rights reserved.
http://dx.doi.org/10.1016/j.bbrc.2013.03.074

chromatin dynamics of pronuclei and epigenetic regulation in the first cell cycle of mouse embryos.

2. Materials and methods

2.1. Oocyte and embryo manipulations

Parp1$^{-/-}$ mutant mice [19] with a B6D2F1 hybrid or C57BL/6J inbred background were used in this study. Oocytes were collected from the superovulated B6D2F1 females 14 hrs after the intraperitoneal injection of pregnant mare serum gonadotropin (PMSG), followed by the injection of human chorionic gonadotropin (hCG). For in vitro fertilization using TYH medium [20], sperm was collected from the caudal epididymis of B6D2F1 males and incubated in TYH medium for at least 30 min for the hyperactivation. The oocyte-cumulus complexes (OCC) were collected from the ampulla of uterine tube of superovulated mice. Sperm (150 sperm/μl) were inseminated in the OCC-containing TYH medium with or without PJ-34 (N-(6-Oxo-5,6-dihydro-phenanthridin-2-yl)-N,N-dimethylacetamide, Alexis Biochemicals) or 5-AIQ (5-aminoisoquinolin-1(2H)-one, Alexis Biochemicals). Intracytoplasmic sperm injection (ICSI) was carried out essentially as described previously [21]. ICSI was carried out in HEPES-buffered CZB medium [22] with or without 30 μM PJ-34. Thereafter, embryos were cultured in modified Whitten medium [23].

2.2. Antibodies

The antibodies and dilutions used in this study are described in Supplemental Table T1. The HRP-conjugated rat or rabbit IgG (1:10,000, Jackson Immunoresearch Laboratory) and HRP-conjugated mouse IgG (1:1000, Bio-RAD) were used as the secondary antibodies and the Alex Fluor conjugates (1:200, Invitrogen) of IgG for immunofluorescence.

2.3. Immunofluorescence

The cumulus-oocyte complex was dissociated by hyarulonidase (Sigma) and the zona pellucida was removed with 0.5% actinase (Kaken, Japan). After incubation of the denuded oocytes or embryos for at least 30 min, the oocytes or embryos were placed into fibrin clots [24]. The fibrin clots were prepared by mixing 1 μl fibrinogen (Calbiochem) with 1 μl thrombin (Sigma). The cells were incubated with primary antibodies for overnight at 4 °C, followed by incubation with blocking buffer (PBS containing 5% normal goat serum and 0.05% Tween-20). The cells were then incubated with secondary antibodies for 1–2 h at 37 °C. After washing with PBS, the cells were counterstained with PI and subjected to microscopic analyses. For the staining of histone modification antibodies, the cells were fixed with 4% paraformaldehyde for 15 min at 4 °C and then permeabilized with PBS containing 0.1% BSA and 0.5% TritonX-100 for 10 min. An immunofluorescence study using 12 kinds of histone acetylation and methylation antibodies was initially carried out using 7–10 embryos to determine the optimum reaction conditions for each antibody. The cells were incubated with primary antibodies overnight at 4 °C, and then with secondary antibodies for at least 3 h at 4 °C. For the staining of DNA methylation, after fixation and permeabilization as described above, embryos were incubated with 2 M HCl for 45 min and then neutralized for 10 min with 100 mM Tris/HCl buffer, pH 8.5. After washing five times with PBS containing 0.05% Tween-20, the embryos were blocked and incubated with anti-5-methylcytosine antibody overnight and incubated with secondary antibody as described above. The DNA was counterstained with DAPI or PI. The images were captured under a light microscopy (Axiophot, Zeiss) or confocal microscopy (IX71 with Fluoview FV300, Olympus) system.

2.4. Two-hybrid screening

Yeast two-hybrid screening was performed with Matchmaker GAL4 Two-hybrid System 3 (Clontech), according to the manufacturer's instructions. Briefly, the cDNA fragments of *ΔParp1* (encoding amino acids 1–739, accession number, NM_007415) were generated by PCR amplification with appropriate primer sequences (Forward, 5′-TGCAGCACGAGAAGGAGG-3′; Reverse; 5′-GTTGACGTCGATGGGATCC-3′). Template cDNA was synthesized from mRNA of mouse ovary or brain using SuperScript III (Invitrogen). The *ΔParp1* was then cloned into the vector pGBKT7. To prepare the cDNA library from MII oocytes, the total RNA was isolated from 100 MII oocytes with Sepasol (Nacalai) according to the manufacturer's instructions. The MII oocyte-derived cDNA was cloned into pGADT7 and bait vectors were co-transfected into the competent yeast strain AH109. The cDNA clones were recovered from nutritionally selected yeast colonies. Confirmation of the interactions in yeast was carried out by co-transfection of the bait vectors and isolated pGADT7 clones (Supplemental Table T2).

2.5. Plasmid preparation and immunoprecipitation

The full-length cDNA encoding Suz12 (NM_199196) was amplified by PCR from cDNA pools derived from mouse ovary or brain (Forward, 5′-GGCCATGGAGGCCACCATGGCGCCTCAGAAGCAC-3′; Reverse, 5′-GGTACCTCAGAGTTTTTGTTTCTTGC-3′). The full-length cDNA encoding Suz12 and *ΔParp1* were cloned into the pCMV-HA and pCMV-Myc mammalian expression vectors (Clontech), respectively. The plasmids were transfected into COS or HEK293T cells by Polyfect transfection reagent (Qiagen), Lipofectamine 2000 (Invitrogen), or the Profection mammalian transfection system (Promega), according to manufacturers' instructions. Forty to 48 h after transfection, the cells were collected into IP lysis buffer (150 mM NaCl, 1% NP-40, 50 mM Tris-HCl (pH 7.5)) or a commercially available lysis buffer (MER buffer (Pierce)), and the lysates were kept at −80 °C. Immunoprecipitation was carried out using the Profound™ Mammalian HA/c-Myc Tag Co-IP kit (Pierce) according to the manufacturer's instructions, or agarose conjugated anti-epitope tag antibodies (MBL). After primary immunoprecipitation with anti-myc agarose, the immunocomplexes were eluted with an elution buffer (pH 2.8, provided by Pierce) and immediately equilibrated with 10 mM Tris-HCl (pH 9.5). Western blots were performed using primary antibodies after SDS-polyacrylamide gel electrophoresis and transfer to Immobilon PVDF membrane (Millipore). Briefly, the membrane was reacted with primary antibodies overnight at 4 °C. The membrane was washed and then incubated with secondary HRP-conjugated antibodies for 2 h at room temperature. The signals were detected with the Chemi-Lumi One kit (Nacalai).

3. Results

3.1. Effects of PARylation on histone modification of the PN embryos

We first examined the effects of PARylation on chromatin modification during postfertilization development using PARP inhibitor PJ-34, because our previous study showed that PJ-34 blocked pronuclear fusion at pronuclear envelop breakdown [17]. In the absence of PJ-34 (untreated embryos), dimethylation of histone H3 at lysine 4 (dimethyl-H3K4) was only observed in the female pronuclei and not in the male pronuclei at 6 h post fertilization (hpf). An upregulation of dimethyl-H3K4 in the male pronuclei at 6 hpf

was detected in the presence of PJ-34 (Fig. 1). The levels of dimethyl-H3K9 were detected in both pronuclei, but down-regulated in both pronuclei in the presence of PJ-34. The level of dimethyl-H3K27 was dominantly observed in female pronuclei at 6 hpf (data not shown) and 15 hpf in the untreated embryos. In contrast, dimethyl-H3K27 was downregulated in the parental pronuclei of PJ-34-treated embryos at 15 hpf (Fig. 1). Western blots also show the upregulation of dimethyl-H3K4 in the PARylation-inhibited embryos at 6 hpf, and downregulation of dimethyl-H3K9 and dimethyl-H3K27 at 15 hpf in the presence of PJ-34 (Fig. 1).

3.2. Physical interaction of Parp1 with Suz12

To elucidate the molecular basis of the effect of PARylation on histone modification, we performed yeast two-hybrid screening using the bait vector carrying the N-terminal and automodification domain of Parp-1, which is the major protein-protein interaction domain, but is lacking the catalytic domain (ΔParp1), because no interactants were obtained through two trials using intact Parp1 bait proteins (data not shown), which may result from ectopic expression/activation of Parp1 toxic in yeast as previously described [25]. Twelve protein candidates interacting with Parp1 were identified (Supplemental Table T2). Among these molecules, we focused on Suz12, a histone methyltransferase in PRC2/3/4 (Polycomb Repressive Complex 2/3/4). Suz12 induces an inactive state of chromatin by modifying histone H3K9 and H3K27 residues. A reciprocal immunoprecipitation study further confirmed the direct interaction of Suz12 with ΔParp1 in HEK293T cells (Fig. 2A).

Immunofluorescence analysis showed Suz12 localized prominently on the spindle of MII oocytes as well as in the ooplasm (Fig. 2B). Notably, in the MII oocytes treated with PJ-34, the signals of Suz12 were hardly detected (Fig. 2D), indicating a possibility that Suz12 may not be stable under deficient PARylation condition. After fertilization, at 6 hpf, Suz12 was mainly detected in both pronuclei, like PAR molecules [17] in the absence of PJ-34 (Fig. 2C). We previously reported that in this stage, Parp1 is localized in pronuclei as well as in ooplasm [17]. PJ-34 treatment disturbed pronuclear fusion as previously reported [17] and reduced the Suz12 immunosignals in the pronuclei and the localization of the

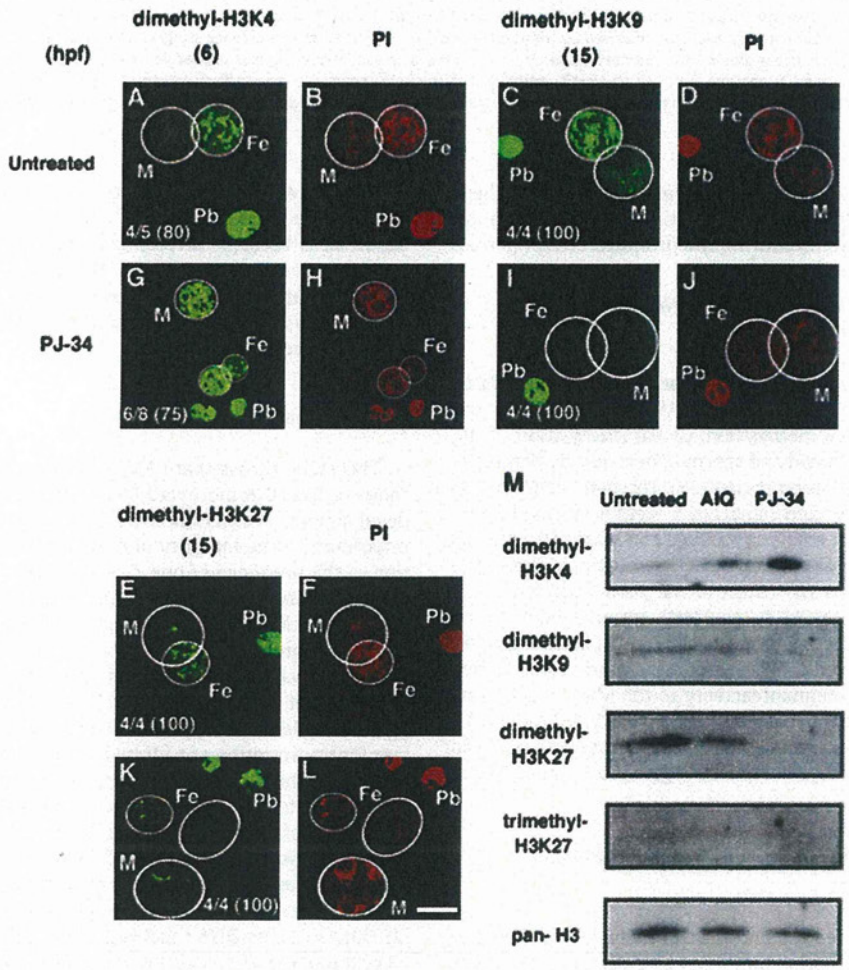

Fig. 1. Analysis of histone modification under PARylation inhibition at the one-cell mouse embryos. Immunofluorescence study with laser-scanning confocal microscopy of untreated (A–F) or 30 μM PJ-34 treated (G–L) one-cell embryos at 6 hpf was performed with antibodies for dimetylated histone H3 at lysine 4 (dimethyl-H3K4), dimethylated histone H3 at lysine 9 (dimethyl-H3K9), dimetylated histone H3 at lysine 27 (dimethyl-H3K27), and is depicted in green. The frequency of the staining patterns and its percentage is given in parenthesis in white (A, C, E, G, I, K). DNA was counterstained with PI (B, D, F, H, J, L). Female (Fe) and male (M) pronuclei (PN), and the nuclei of polar body (Pb) are indicated. Circles (white lines) indicate the outlines of PN. (M) Western blots were performed with crude extracts corresponding to 100 PN embryos with antibodies against dimethyl-H3K4, dimethyl-H3K9, dimethyl-H3K27, trimetylated histone H3 at lysine 27 (trimethyl-H3K27), and unmodified histone H3 (pan-H3). Bar represents 25 μm. (For interpretation of color in Figure, the reader is referred to the web version of this article).

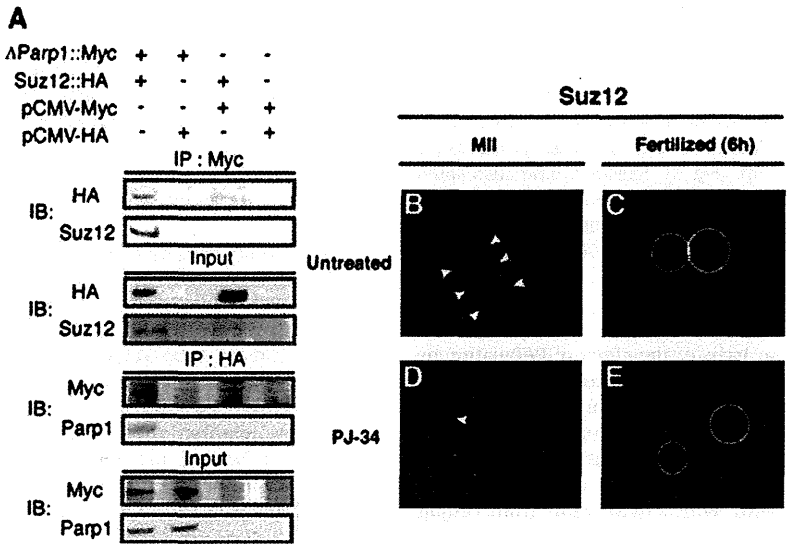

Fig. 2. Interaction of Parp1 with Suz12 in vitro and localization of Suz12 in the PN of mouse one-cell embryos. Extracts from HEK293T cells transfected with combinations of plasmids carrying mouse Parp1 lacking the catalytic domain (ΔParp1) tagged with Myc (ΔParp1::Myc), intact Suz12 tagged with HA (Suz12::HA), and mock plasmids (CMV-Myc, CMV-HA) were used for immunoprecipitation (IP) followed by immunoblotting (IB) (A). Immunofluorescence study of MII oocytes (B and D), or one-cell embryos at 6 hpf (C and E). Detected antigens appear green. DNA counterstained by PI is colored with red. Merged signals appear yellow or orange. Arrowheads indicate the spindle structure (B) and MII chromosome (D) positive for the anti-Suz12 antibody. White circle represents the outline of pronuclei (C and E). The frequency (percentage in parenthesis) of staining patterns was indicated in each panel (B–E). Bar represents 10 μm. (For interpretation of color in Figure, the reader is referred to the web version of this article).

immunosignals in the ooplasm is slightly increased (Fig. 2E). These results suggest that PARylation is required for proper localization of Suz12 on the chromosomes during the pronuclei fusion period.

3.3. Hypomethylation of maternal gamete DNA by PARylation inhibition

Recently, functional links between histone methylation and DNA methylation have been elucidated [26,27]. We next sought for the roles of PARylation in DNA methylation. Global methylation of the maternal genome is maintained and sperm DNA is quickly demethylated during the postfertilization period [28]. Through our immunofluorescence study we detected signals of 5-methylcytosine (MetC) in the female pronuclei of embryos produced by in vitro fertilization (IVF) and both pronuclei of parthenogenetic embryos at 6 hpf/post-activation (hpa), as well as the nuclei of the polar bodies (Fig. 3A and B). By incubation with PJ-34, the MetC-immunoreactivity became almost absent in both pronuclei of IVF and parthenogenetic embryos (Fig. 3C and D), indicating the robust hypomethylation of female pronuclei. The low immunoreactivity to the MetC antibody in the PJ-34 treated embryos persisted at least until 15 hpf with PJ-34 in the culture medium (data not shown). These results indicate that PARylation is involved in the maintenance of global DNA methylation of female pronuclei.

3.4. Disorganized chromatin ultrastructure under PARylation inhibition in the pronuclei

We further investigated the chromatin organization of the pronuclei and effects by PARylation inhibition by electron microscopy (EM). Rosette-like structure of electron-dense areas was detected in the female pronuclei of untreated one-cell embryos at 6 and 15 hpf (Fig. 3). Such electron-dense areas were not detected in male pronuclei at 6 hpf but appeared at 15 hpf (Fig. 3I–K). With PJ-34 treatment, electron-dense areas are increasingly detectable in the female pronuclei, but not in the male pronuclei at 6 hpf (Fig. 3K–T). At 15 hpf, uncharacterized structure with a high electron-density was observed in female pronuclei and the electron-dense areas became increasingly detectable also in the male pronuclei in the presence of PJ-34 (Fig. 2S and T). It is thus suggested that PARylation inhibition induces rosette-like electron-dense areas corresponding to disorganized hypercondensed chromatin in the pronuclei.

4. Discussion

This study shows that PARylation regulates methylation of histone H3 and DNA methylation during the first cell cycle of mouse development. Furthermore, our data suggests that PARylation is important for the integrity of non-equivalent chromatin organization of the pronuclei of one-cell embryos.

Our observation of global upregulation of dimethyl-H3K4 and downregulation of both dimethyl-H3K9 and dimethyl-H3K27 suggests that chromatin modification during the first cell-cycle seems to shift toward global transcription activation under a normal development (Fig. 4). This mechanism should be important for genome-wide transcriptional upregulation, but is likely not important for transcription of a limited number of genes expressed at the one-cell embryos, whose expression is indispensable for further development. We speculate that PARylation is required for proper conversion of parental genomes during one-cell stage prior to the global activation of the zygotic genome that takes place at the two-cell stage. Roles of PARylation in histone modification regulation have been shown to involve both transcription and replication [29,30] as well as DNA repair and recombination [31]. In addition, PARylation affects relaxation of chromatin structure in vitro [32] and in vivo [33], which may be mediated by PARylation of Parp1 itself or histone H1. Our findings provide a unique biological window to elucidate the regulation of PARylation on chromatin ultrastructure in mammalian development (Fig. 4).

Our findings also demonstrate that PARylation acts as regulatory machinery for the methylation of histone H3 (Fig. 4). Aberrant

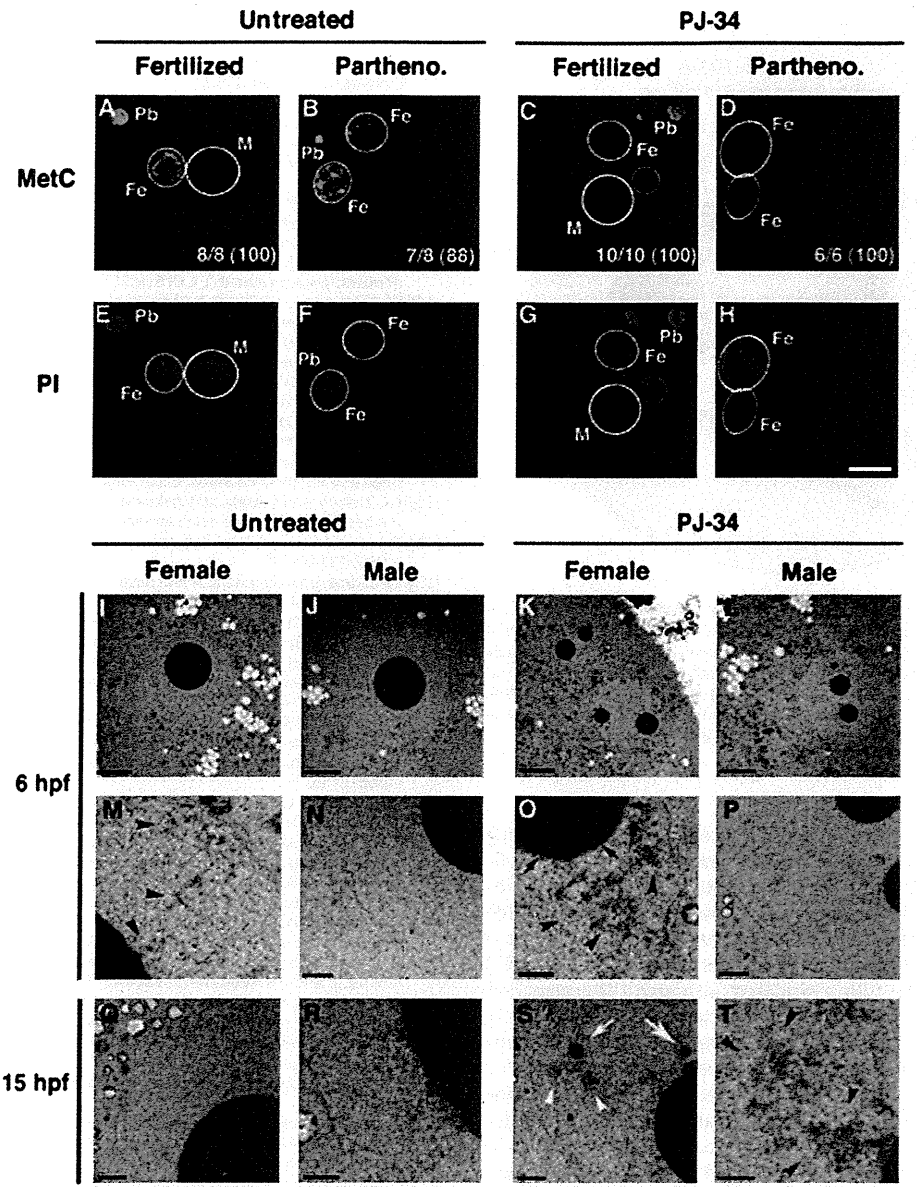

Fig. 3. Effects of PARylation inhibition on DNA methylation and ultrastructure of pronuclear organization by electron microscopy. Laser scanning confocal immunofluorescence study using IVF (fertilized; A and C) and parthenogenetic (parthenotes; B and D) embryos at 6 hpf. Embryos were cultured under normal conditions (A and B) and PJ-34 (30 μM) added 1 h before insemination or Sr^{2+}-activation (C and D). Signals of antibody for 5-methylcytosine (MetC) were colored with green. DNA counterstained with PI was colored in red (E–H). White circle represents the outlines of female (Fe) and male (M) pronuclei. Other PI signals represent DNA in the polar body (Pb). Values (percentage in parenthesis) represent frequency of staining patterns in each panel (A–D). EM observation of pronuclei in embryos at 6 hpf (I–P) and 15 hpf (Q–T) is shown in Fig 3I T. Rosette-like structures of electron-dense areas were detected in untreated female pronuclei at 6 hpf (arrowheads in M). The dense areas were increased by PARylation inhibition (arrowheads in O). Ambiguous outlines of pronuclear membrane were observed in PJ-34-treated embryos (arrows in O). Uncharacterized electron-dense structures were detected in female pronuclei with PARylation inhibition (white arrows and arrowheads in S). Rosette-like structures appeared in the male pronuclei of PJ-34-treated embryos (arrowheads in T). Bars represent 10 μm (I–L) and 5 μm (M–T). (For interpretation of color in Figure, the reader is referred to the web version of this article).

localization of Suz12, a histone methyltransferase, by PJ-34 may be related to the decrease of di-methylation of histone H3K9 and K27 in the female pronuclei. Suz12 is a component of PRC2/3/4, which regulates the repressive status of transcription by the methylation of histone H3K9 and H3K27 [34]. Our findings support the idea that Parp1 acts as a regulatory scaffold for the access of PRC2/3/4 to target DNA, because none of the components of the PRC2/3/4 complexes are DNA binding proteins. We previously observed Parp1, 2, 3, 6, 7, 8, 9, 12, 16 and Tans1 and 2 mRNAs are expressed in the mouse oocytes [17]. Further analyses are needed to identify the responsible methyltranferases for histone H3K4 methylation, which are regulated by PARylation by particular PARP family member(s) during early stages of postfertilization development.

An additional conclusion of this finding is that PARylation regulates the epigenetic nonequivalence of the pronuclei in embryos (Fig. 4). The molecular mechanisms regulating the asymmetric DNA methylation of one-cell embryos are largely unknown. We were able to contribute to delineation of the mechanisms by show-

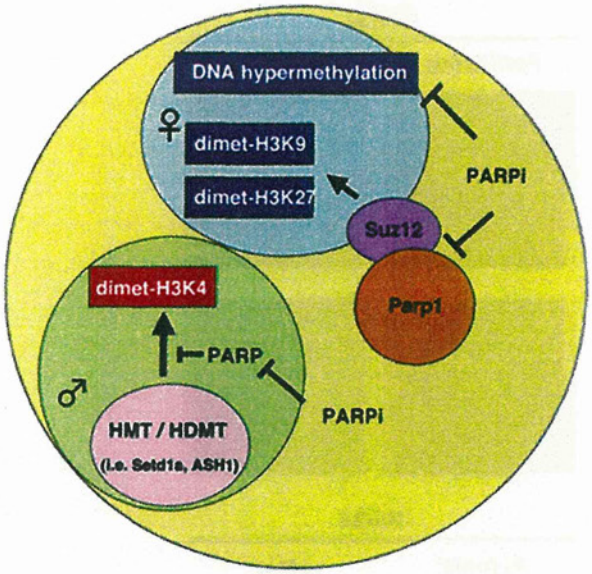

Fig. 4. Scheme of putative roles of PARylation in the chromatin dynamics of one-cell embryos. The Parp1-Suz12 complex may, in parts, regulate the H3K9 or H3K27 status of the female pronuclear genome. Hypermethylation status of female pronuclei may be regulated by the Dnmt1-Parp1 complex or other interactants of Parp1 including demethylases. On the other hand, H3K4 methylation of paternal pronuclei may be regulated by the interaction of PARP family member(s) and particular H3K4 methyltransferases present in oocytes through PARylation.

ing that PARylation is involved in the epigenetic regulation during early development in mice. PGC7/Stella-deficient eggs show similar defects in the protection of female pronuclei from DNA demethylation [35]. The nucleo-cytoplasmic transport of the responsible proteins appears to be important for the regulation of DNA methylation. The role of PARylation in DNA methyltransferase (DMNT) regulation is yet to be fully elucidated, although the interaction of DNMT1 with Parp1 and the indirect repression of DNMT1 activity by interacting with PAR have been suggested [36]. It is speculated that PARylation regulates the accessibility of DNMT or demethylase to DNA, in a manner mediated by chromatin remodeling. It is also of interest that PAR may participate in demethylation regulation by Gadd45a, involving base-excision repair, in which Parp1 and Parg also play important roles [37]. Our study provides a novel avenue for better understanding of establishment of chromatin organization through the histone codes, and DNA methylation with PARylation that may underlie at the beginning of zygotic development.

Acknowledgments

We would like to thank Hideki Ogino and for their technical assistance. We are grateful for Ryuzo Yanagimachi, Toshiaki Noce and Takashi Sugimura for discussion and suggestions. A. R. is a JSPS fellow.

This work was supported in part by a Grant-in-Aid from MEXT and the Third Term Comprehensive 10-Year Strategy for Cancer Control, National Cancer Center Research.

Appendix A. Supplementary data

Supplementary data associated with this article can be found, in the online version, at **http://dx.doi.org/10.1016/j.bbrc.2013.03.074.**

References

[1] T. Sugimura, M. Miwa, Poly(ADP-ribose): historical perspective, Mol. Cell. Biochem. 138 (1994) 5–12.
[2] V. Schreiber, F. Dantzer, J.C. Ame, G. de Murcia, Poly(ADP-ribose): novel functions for an old molecule, Nat. Rev. Mol. Cell Biol. 7 (2006) 517–528.
[3] D. D'Amours, S. Desnoyers, I. D'Silva, G.G. Poirier, Poly(ADP-ribosyl)ation reactions in the regulation of nuclear functions, Biochem. J. 342 (1999) 249–268.
[4] A.J. Gottschalk, G. Timinszky, S.E. Kong, et al., Poly(ADP-ribosyl)ation directs recruitment and activation of an ATP-dependent chromatin remodeler, Proc. Natl. Acad. Sci. USA 106 (2009) 13770–13774.
[5] M. Rouleau, R.A. Aubin, G.G. Poirier, Poly(ADP-ribosyl)ated chromatin domains: access granted, J. Cell Sci. 117 (2004) 815–825.
[6] G. Timinszky, S. Till, P.O. Hassa, et al., A macrodomain-containing histone rearranges chromatin upon sensing PARP1 activation, Nat. Struct. Mol. Biol. 16 (2009) 923–929.
[7] R. Krishnakumar, M.J. Gamble, K.M. Frizzell, et al., Reciprocal binding of PARP-1 and histone H1 at promoters specifies transcriptional outcomes, Science 319 (2008) 819–821.
[8] H.L. Liu, K.T. Hara, F. Aoki, Role of the first mitosis in the remodeling of the parental genomes in mouse embryos, Cell Res. 15 (2005) 127–132.
[9] C. Bouniol, E. Nguyen, P. Debey, Endogenous transcription occurs at the 1-cell stage in the mouse embryos, Exp. Cell Res. 218 (1995) 57–62.
[10] C.C. Henery, M. Miranda, M. Wiekowski, et al., Repression of gene expression at the beginning of mouse development, Dev. Biol. 169 (1995) 448–460.
[11] R.M. Schultz, Regulation of zygotic gene activation in the mouse, BioEssay 15 (1993) 531–538.
[12] W. Tadros, H.D. Lipshitz, The maternal-to-zygotic transition: a play in two acts, Development 136 (2009) 3033–3042.
[13] R.M. Schultz, The molecular foundations of the maternal to zygotic transition in the preimplantation embryo, Hum. Reprod. Update 8 (2002) 323–331.
[14] D.W. McKay, H.J. Clarke, The ability to organize sperm DNA into functional chromatin is acquired during meiotic maturation in murine oocytes, Dev. Biol. 186 (1997) 73–84.
[15] G.T. Williams, S. Shall, C.C. Ford, NAD turnover during early development of Xenopus laevis, Biochim. Biophys. Acta 762 (1983) 272–280.
[16] D. Epel, The initiation of development at fertilization, Cell Differ. Dev. 29 (1990) 1–12.
[17] T. Osada, H. Ogino, T. Hino, et al., PolyADP-ribosylation is required for pronuclear fusion during postfertilization in mice, PLoS One 5 (2010) e12526.
[18] T. Osada, M. Masutani, PolyADP-ribosylation in postfertilization and genome reprogramming: implications for carcinogenesis, in: Gomes, A.D.S. Gomes (Eds.), Polymerization, InTech, New York, 2012. 10.5772/46097.
[19] M. Masutani, H. Suzuki, N. Kamada, et al., Poly(ADP-ribose) polymerase gene disruption conferred mice resistant to streptozotocin-induced diabetes, Proc. Natl. Acad. Sci. USA 96 (1999) 2301–2304.
[20] Y. Toyoda, M. Yokoyama, T. Hoshi, Studies on the fertilization of mouse eggs in vitro, J. Anim. Reprod. 16 (1971) 147–151.
[21] T. Osada, A. Toyoda, S. Moisyadi, et al., Production of inbred and hybrid transgenic mice carrying lathe (>200 kb) foreign DNA fragments by intracytoplasmic sperm injection, Mol. Reprod. Dev. 72 (2005) 329–335.
[22] M.C. Summers, L.K. McGinnis, J.A. Lawitts, et al., IVF of mouse ova in a simplex optimized medium supplemented with amino acids, Hum. Reprod. 15 (2000) 1791–1801.
[23] W.K. Whitten, J.D. Biggers, Complete development in vitro of the pre-implantation stages of the mouse in a simple chemically defined medium, J. Reprod. Fertil. 17 (1968) 399–401.
[24] C. Simerly, G. Schatten, Techniques for localization of specific molecules in oocytes and embryos, Methods Enzymol. 225 (1993) 516–553.
[25] E. Perkins, D. Sun, A. Nguyeb, et al., Novel inhibitors of poly(ADP-ribose) polymerase/PARP1 and PARP2 identified using a cell-based screen in yeast, Cancer Res. 61 (2001) 4175–4183.
[26] F.E. Erfurth, R. Popovic, J. Grembecka, et al., MLL protects CpG clusters from methylation within the Hoxa9 gene, maintaining transcript expression, Proc. Natl. Acad. Sci. USA 105 (2008) 7517–7522.
[27] T. Vaissiere, C. Swan, Z. Herceg, Epigenetic interplay between histone modification and DNA methylation in gene silencing, Mutat. Res. 659 (2008) 40–48.
[28] W. Mayer, A. Niveleau, J. Walter, et al., Demethylation of the zygotic paternal genome, Nature 402 (2000) 501–502.
[29] D. Quenet, V. Gasser, L. Fouillen, et al., The histone subcode: poly(ADP-ribose) polymerase-1 (Parp-1) and Parp-2 control cell differentiation by regulating the transfcriptional intermediary factor TIF beta and heterochromatin protein HP1alpha, FASEB J. 22 (2008) 3853–3865.
[30] T. Boulikas, Poly(ADP-ribosylated) histones in chromatin replication, J. Biol. Chem. 265 (1980) 14638–14647.
[31] A. Huber, P. Bai, M. de Murcia, et al., PARP-1, PARP-2 and ATM in the DNA damage response: functional synergy in mouse development, DNA Repair 3 (2004) 1103–1108.
[32] G.G. Poirier, G. de Murcia, J. Jongstra-Bilen, et al., Poly(ADP-ribosyl)ation of polynucleosomes causes relaxation of chromatin structure, Proc. Acad. Natl. Sci. USA 79 (1982) 3423–3427.
[33] A. Tulin, A. Spradling, Chromatin loosening by poly(ADP)-ribose polymerase (PARP) at Drosophila puff loci, Science 299 (2003) 560–562.

[34] R. Cao, Y. Zhang, SUZ12 is required for both the histone methyltransferase activity and the silencing function of the EED-EZH2 complex, Mol. Cell 2 (2004) 57–67.
[35] T. Nakamura, Y. Arai, H. Umehara, et al., PGC/Stella protects against demethylation in early embryogenesis, Nat. Cell Biol. 9 (2007) 64–71.
[36] P. Caiafa, T. Guastafierro, M. Zampieri, Epigenetics: poly(ADP-ribosyl)ation of PARP-1 regulates genomic methylation patterns, FASEB J. 23 (2009) 672–678.
[37] G. Barreto, A. Schafer, J. Marhold, et al., Gadd45a promotes epigenetic gene activation by repair-mediated DNA demethylation, Nature 445 (2007) 671–675.

THE JOURNAL OF BIOLOGICAL CHEMISTRY VOL. 287, NO. 44, pp. 36777–36791, October 26, 2012

Induction of Cancerous Stem Cells during Embryonic Stem Cell Differentiation*[S]

Received for publication, April 17, 2012, and in revised form, August 30, 2012 Published, JBC Papers in Press, September 7, 2012, DOI 10.1074/jbc.M112.372557

Hiroaki Fujimori[‡§], Mima Shikanai[§], Hirobumi Teraoka[§], Mitsuko Masutani[‡], and Ken-ichi Yoshioka[‡§1]

From the [‡]Division of Genome Stability Research, National Cancer Center Research Institute, 5-1-1 Tsukiji, Chuo-ku, Tokyo 104-0045, Japan and the [§]Department of Pathological Biochemistry, Medical Research Institute, Tokyo Medical and Dental University, 2-3-10 Kandasurugadai, Chiyoda-ku, Tokyo 101-0062, Japan

Background: Cancer stem cells are responsible for tumorigenesis; however, the developmental process is poorly understood.
Results: Differentiating stem cells in aberrant environments are subjected to carcinogenic stress, leading to genomic instabilization, mutation inductions, and cellular transformation with stemness characteristics.
Conclusion: Aberrant environment for differentiation risks cancerous stem cell development.
Significance: This is the first report showing normal stem cell transformation into malignant counterparts and their process.

Stem cell maintenance depends on their surrounding microenvironment, and aberrancies in the environment have been associated with tumorigenesis. However, it remains to be elucidated whether an environmental aberrancy can act as a carcinogenic stress for cellular transformation of differentiating stem cells into cancer stem cells. Here, utilizing mouse embryonic stem cells as a model, it was illustrated that environmental aberrancy during differentiation leads to the emergence of pluripotent cells showing cancerous characteristics. Analogous to precancerous stages, DNA lesions were spontaneously accumulated during embryonic stem cell differentiation under aberrational environments, which activates barrier responses such as senescence and apoptosis. However, overwhelming such barrier responses, piled-up spheres were subsequently induced from the previously senescent cells. The sphere cells exhibit aneuploidy and dysfunction of the *Arf-p53* module as well as enhanced tumorigenicity and a strong self-renewal capacity, suggesting development of cancerous stem cells. Our current study suggests that stem cells differentiating in an aberrational environment are at risk of cellular transformation into malignant counterparts.

A tumor consists of a heterogeneous cell mass in which only a small portion of the malignant cells, *i.e.* cancer stem cells (CSCs),[2] are responsible for tumor initiation and propagation (1). In fact, CSCs identified in a variety of tumors demonstrate a capacity for self-renewal and differentiation, which is shared by normal stem cells (2). Although cancer stem-like cells can be induced from stem/progenitor as well as differentiated cells by oncogene overexpression (3, 4), it remains unclear how CSCs spontaneously develop.

In the initial stages of carcinogenesis cells accumulate DNA replication stress-associated lesions that are induced by aberrant growth acceleration or oncogene activation, resulting in the activation of barrier reactions for carcinogenesis such as cell cycle arrest, senescence, and apoptosis (5, 6). These cellular responses illustrate the competing forces of cancer progression and prevention. Genomic instability is invariably accompanied with these stages of cancer development (6, 7). Analogously, mouse embryonic fibroblasts (MEFs) can escape senescence and exhibit immortality through accumulation of DNA replication stress-associated lesions under continuous growth acceleration, which accompanies genomic instability (8) and *Arf/p53* mutations (9). However, unlike CSCs, immortalized MEFs show neither tumorigenicity nor stemness characteristics (10).

The difference between immortal MEFs and CSCs underlies the properties of stemness characteristics. In addition to the expression of undifferentiated marker genes, both somatic stem cells and CSCs show sphere-formation abilities and heightened expression of the ATP binding cassette transporter and glycolysis dependence (11, 12). Importantly, whereas these properties are widely observed in stem cells, including embryonic stem cells (ESCs) (13–16), immortal MEFs do not acquire such properties during immortalization. Unlike immortal MEFs, CSCs share specific profiles of cell-surface antigens with somatic stem cells (11). However, like immortal MEFs, CSCs also show genomic instability and mutations, which are unshared characteristics with normal stem cells (17).

The existing body of literature on stem cells suggests that carcinogenesis can be initiated in somatic stem cells when the cells are subjected to the same conditions of stress that induce MEF immortalization. However, this challenges the idea of stem cell homeostasis, which is strongly protected by niche environments from the induction of genomic instability and

* This work was supported, in whole or in part, by Ministry of Education, Culture, Sports, Science, and Technology of Japan KAKENHI (20770136, 20659047), Grant-in-aid and the Third Term Comprehensive 10-Year Strategy for Cancer Control (10103833), and the National Cancer Center Research and Development Fund (23-C-10).
[S] This article contains supplemental Tables 1 and 2 and Figs. S1–S5.
[1] To whom correspondence should be addressed. Tel.: 81-3-3542-2511; Fax: 81-3-3543-9305; E-mail: kyoshiok@ncc.go.jp.
[2] The abbreviations used are: CSC, cancer stem cell; MEF, mouse embryonic fibroblast; ESC, embryonic stem cell; EB, embryoid body; NBS, newborn bovine serum; ABS, adult bovine serum; HU, hydroxyurea; iIC, induced immortal-like cell; NCS, neocarzinostatin; cGC, continuously growing cell; PARP, poly(ADP-ribose) polymerase; KSR, knockout serum replacement; LIF, mouse leukemia inhibitory factor.

transformation (18). In agreement with this argument, stem cells injected into heterotropic sites are strongly implicated in tumorigenesis, in association with environmental aberrancies for stem cell maintenance (19). Further supporting the notion of stem cell tumorigenicity in aberrant environments, embryonal carcinomas were developed from xenografts of inner cell masses from mouse blastocyst and derailed primordial germ cells from the migration track (20, 21). Moreover, a recent study suggested that oncogenesis could be triggered by a niche disruption, resulting in disordered differentiation (22).

Taken together with a report showing stem cell niche dysfunction as a result of aging (23), these studies motivated the hypothesis that differentiating stem cells can become CSCs upon exposure to carcinogenic stress in a process analogous to MEF immortalization.

MATERIALS AND METHODS

Cell Culture—Culture of mouse ESCs and embryoid body (EB) formation assays were performed as previously described (24). For differentiation, cloned ESCs maintained with Knock-Out Serum Replacement (Invitrogen) and ESGRO (mouse leukemia inhibitory factor (LIF); Millipore, Billerica, MA) were cultured in three kinds of medium consisting of Iscove's modified Dulbecco's medium (Invitrogen) supplemented with FBS (Invitrogen), newborn bovine serum (NBS; Sigma), or adult bovine serum (ABS; Invitrogen) at 20%. The piled-up spheres were stained by crystal violet (Sigma), and the number of spheres was counted. Populations at P6 + 14 days were harvested by employing 0.25% trypsin-EDTA (Invitrogen) and then cultured in each medium for further experiments. All the following experiments were performed using bulk populations without cloning. Primary MEF immortalization assays were performed as previously described (8). For detection of the phenotype with an abnormal p53 pathway, each population was cultured in medium containing hydroxyurea (HU) as previously described (25). Sphere formation assay was performed as previously described (26) with a little modification. Briefly, CD133-positive and -negative populations were seeded to NBS-med containing methylcellulose 4000 (Wako, Tokyo, Japan) for 4 days. For detection, spheres were attached to culture dishes and were stained by crystal violet after 2 days of attachment (Sigma).

β-Galactosidase Activity Detection—β-Galactosidase activity was detected as previously described (27). Briefly, cultured cells were fixed with 4% formaldehyde and then incubated in staining buffer (1 mg/ml 5-bromo-4-chloro-3-indolyl-β-D-galactopyranoside (X-gal), 5 mM $K_3Fe(CN)_6$, 5 mM $K_4Fe(CN)_6$, and 2 mM $MgCl_2$ in PBS).

Reverse Transcription-Polymerase Chain Reaction—RT-PCR and quantified RT-PCR were performed as described (24). Briefly, total RNA was extracted from cultured cells with an RNeasy kit (Qiagen, Tokyo, Japan) and treated with DNase I (Promega, Tokyo, Japan). cDNAs were synthesized from 1 μg of total RNA using Super Script III first-strand synthesis system (Invitrogen). Ampli Taq Gold PCR Master Mix (Invitrogen) or Power SYBR Green PCR Master Mix (Invitrogen) was employed for PCR reaction. The primer list is described in supplemental Table 1.

Antibodies, Immunostaining and Western Blotting—The antibodies used are listed in supplemental Table 2. Immunostaining and Western blot analysis were performed as previously described (8). Briefly, for Western blotting, proteins were transferred onto a nitrocellulose membrane and probed with appropriate primary antibodies. The membrane was incubated with corresponding secondary antibodies conjugated with horseradish peroxidase, and the antigen-antibody complex was visualized by Immobilon Western (Millipore). For immunostaining, cells were fixed with formalin and then treated with Triton X-100. After blocking with serum, they were incubated with each primary antibody and then detected with fluorescent secondary antibodies.

Chromosomal Instability Detection—Giemsa staining and flow cytometric analysis were performed as previously described (8). Briefly, mitotic cells prepared by nocodazole treatment were hypotonically swollen with 75 mM KCl and then fixed with Carnoy's solution (75% methanol, 25% acetic acid). They were stained with 4% Giemsa (Merck) solution.

Apoptosis Detection Assay—Terminal deoxynucleotidyl-transferase-mediated dUTP-biotin nick-end labeling (TUNEL) was performed with the *in situ* Apoptosis Detection kit (Takara Bio, Otsu, Japan). The TUNEL-positive cells were detected by FACSCalibur HG (BD Biosciences). The sub-G_1 population was quantified as previously described (28).

Detection of p53 Mutation—The p53 transcripts from each population were amplified from the cDNA from each population and cloned using the pGEM-Easy vector system (Promega), and then the clones were sequenced by an ABI PRISM 3700 DNA analyzer (Invitrogen).

Tumor Formation Assay—For the tumor formation assay, 10^6 cells suspended in 100 μl of serum-free medium were mixed with an equal-volume of growth factor-reduced Matrigel (BD Biosciences) and injected subcutaneously into NOD.CB17-Prkdc^{scid}/J (NOD-SCID) mice. Tumor weight was measured 4 weeks after injection. Tumors were dissolved by dispase (Invitrogen) in part, and total RNA was extracted.

Isolation of CD133-positive Cells—CD133 positive fractions of induced immortal-like cells (iICs) in NBS-med were isolated by a magnetic bead cell sorting or fluorescence activated cell sorting (FACS) technique as previously described (24, 29). Briefly, for magnetic bead cell sorting, Dynabeads (Invitrogen) were coated with CD133 antibody (eBioscience). The beads/antibody complexes were incubated with cells, then the CD133-positive fraction was collected by a magnetic particle concentrator (Invitrogen). RNA was extracted from CD133-positive and -negative populations and subjected to RT-PCR. For FACS, cells incubated with CD133 antibody conjugated with Alexa Fluor 488 were sorted by FACS Aria II system (BD Biosciences). CD133-positive and negative fractions were subjected to sphere formation assay. Details of employed antibodies are described in supplemental Table 2.

Chemical Treatment of Differentiating Cells—The differentiating cells 1 day after passage 3 in ABS medium were treated with 25, 75, or 200 ng/ml neocarzinostatin (NCS). After 1 day, cells were passaged with NCS(+) medium. After 3 days, medium was changed to NCS(−) medium. This procedure is illustrated in Fig. 4*E*.

For Akt or PARP inhibition, differentiating cells on P2 or P1 cells in NBS-med were subjected to 0.25 μM Akt inhibitor IV (Merck) for 4 days or 0.5 μM AZD2281 (Selleck Chemicals, Houston, TX) for 6 days, respectively. These procedures are illustrated in Fig. 8*A*. Cell numbers and the ratio of live/dead cells were calculated by a TC10 automatic cell counter (Bio-Rad).

Statistical Analysis—All statistical analyses were performed using at least three independent measurements. All error bars represent S.D. ($n - 1$). Analysis of variance followed by Bonferroni multiple comparison test (see Figs. 1*F* and 6*A*) or *t* test with Welch correction (see Figs. 2*G*, 4*D*, 6*C*, 6D*c*, 6*F*, 6*G*, and 7*B* and **supplemental Figs. S4*D* and S5**) was performed for assessment. *p* values <0.05 were considered to be significant. The *green asterisks* on Fig. 6*C* and 6*Dc* and **supplemental Figs. S4*D* and S5** indicate significant differences in value between each sample and ESCs.

RESULTS

ESCs Differentiating in an Aberrant Environment Senesce After Serial Proliferation, Leading to the Development of Immortalized Sphere Colonies—To directly address whether differentiating stem cells in aberrant environments are subjected to stress for cellular transformation, the effects of changes in the differentiation culture conditions of ESCs were first assessed. Although ESC injection under a homotopic implantation into blastocysts shows normal embryogenesis, that under heterotopic transplantations leads to tumor development (teratomas or teratocarcinomas) (20). Based on this, we attempted to construct an *in vitro* model in which ESCs maintained with KSR/LIF medium were subjected to differentiation in the medium containing FBS-med, NBS-med, or ABS-med (Fig. 1*A*). Differentiating cells were passaged under unique ESC passage conditions to produce consistent cellular environments. As shown in Fig. 1*B*, ESCs differentiating under each condition initially grew but then stopped proliferation, showing altered morphologies while differentiating (Fig. 1*B*, *P3* and *P5 cells*, *arrows*). Cells in NBS-med typically become senescent, as demonstrated by their flattened and enlarged morphology and senescence-associated β-galactosidase activation (Fig. 1*C*). Such senescent cells were first observed at P3 and became dominant in the culture at P5 (Fig. 1*B*, *P3* and *P5*, *arrows*).

Surprisingly, analogous to MEF immortalization, continuous cultivation in NBS-med led to the emergence of re-proliferating colonies in the previously senescent cells (Fig. 1, *B* (see *panels NBS* at *P6 + 14 days*) and *D*). Because these proliferating cells were able to continuously proliferate more than 40 passages in an immortal manner (data not shown), we named them "induced immortal-like cells" (iICs). Intriguingly, iICs appeared with piled-up sphere morphology in LIF-free medium containing NBS (Fig. 1*D*). Whereas cultivation in FBS-med conditions also, subsequently, led to a small subset of continuously growing cells (cGCs) without showing a canonical senescent stage, piled-up colonies were rarely observed in FBS-med and ABS-med (Fig. 1*B*; *P6 + 14 days*, *E*, and *F*), suggesting that piled-up sphere development through senescence is dependent on differentiation culture conditions. Similar to MEF immortalization (Fig. 1*G*), differentiating ESCs in NBS-med first senesced and then spontaneously developed re-proliferating cells. However, unlike immortalized MEFs, ESCs in NBS-med subsequently formed piled-up spheres that are characteristic of stem cells, suggesting that the induced colonies, in fact, are cancerous transformants possessing stemness characteristics.

iICs in NBS-med Show Cancerous Characteristics—To determine whether the iICs, appearing in aggregates of sphere colonies, exhibited cancerous features, the cells were first assessed for genomic instability, which is a characteristic of cancer cells (30). As expected, the iICs showed aneuploidy, most of which is a common type of genomic instability in cancer cells, at P6 + 14 days in Giemsa staining of spread chromosomes (Fig. 2*A*) and in DNA content analysis using flow cytometry (Fig. 2*B*). Thus, the development of genomic instability accompanies immortal sphere formation in ESC-derived differentiating cells in NBS-med in a process analogous to carcinogenesis.

Because most cancer cells are mutated in either *Arf* or *p53* in a mutually exclusive manner and lose the function of Arf-dependent p53 activation (31), the mutation status of *p53* in the iICs in NBS-med was determined. In contrast to the original ESCs, *p53* mutations were observed in the iICs in as many as 7 of 10 transcripts, including six independent mutations (Fig. 2*C*). Next, to determine the status of functional loss of the *Arf*/*p53* pathway, p53-mediated senescence-like arrest was investigated using treatment with a low dose of HU, which induces DNA replication stress but allows continuous proliferation in *p53*-mutated populations (25). Although the cGCs in FBS-med as well as primary MEFs were completely arrested by HU treatment (**supplemental Fig. S1C**), the iICs in NBS-med still proliferated under HU treatment conditions (Fig. 2, *D* and *E*), suggesting p53 dysfunction. Taken together, our results demonstrated that iICs in NBS-med show genomic instability and functional loss of the p53 pathway. However, such properties of genomic instability and p53 dysfunction have been observed even in non-tumorigenic immortal MEFs (9), posing a question on the tumorigenicity of cancerous characteristics.

When iICs in NBS-med were injected into NOD-SCID mice, the resulting tumors were significantly larger compared with the original ESCs (Fig. 2*F*), indicating increased tumorigenicity of the iICs in NBS-med. Thus, our results together suggested that the iICs in NBS-med were indeed cancerous cells. Whereas genomic instability and mutations in the *Arf*/*p53* module were also observed in immortalized MEFs, further tumorigenicity is a feature unique to CSCs. Therefore, unlike immortal MEFs, the iICs in NBS-med derived from ESCs might accompany the acquisition of stemness characteristics.

iICs in NBS-med Show Properties of Stem Cells—Stem cell properties are represented by the expression of stemness marker genes and the capacity for self-renewal and differentiation, which are shared by somatic stem cells, ESCs and CSCs (2). The iICs in NBS-med showed strong expression of the pluripotent marker genes (*Klf4*, *Nanog*, and *Oct3/4*) and of the differentiation marker gene *CD133* along with weak expression of *Cdx2* and *T* (Fig. 3*A*), indicating that the iICs in NBS-med

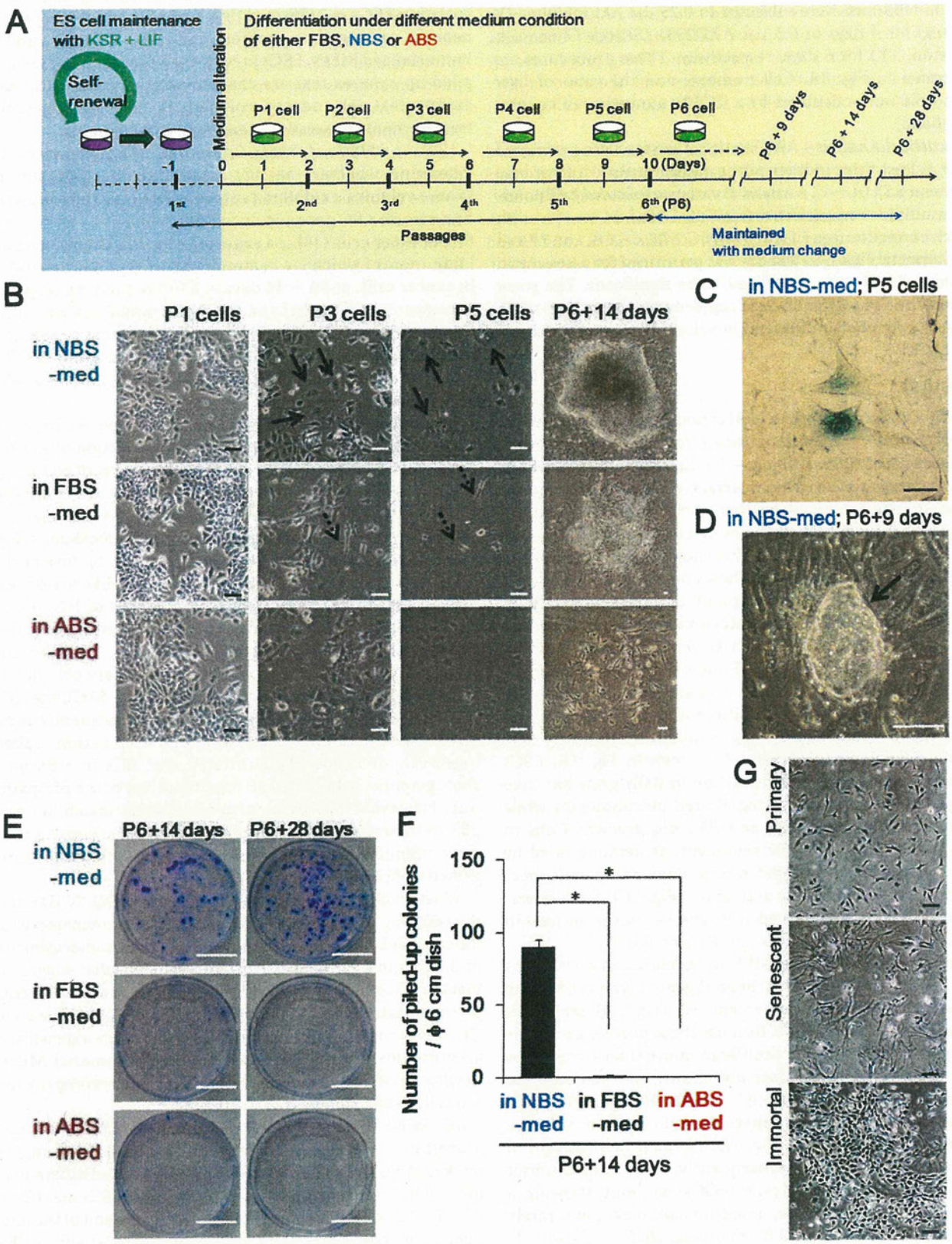

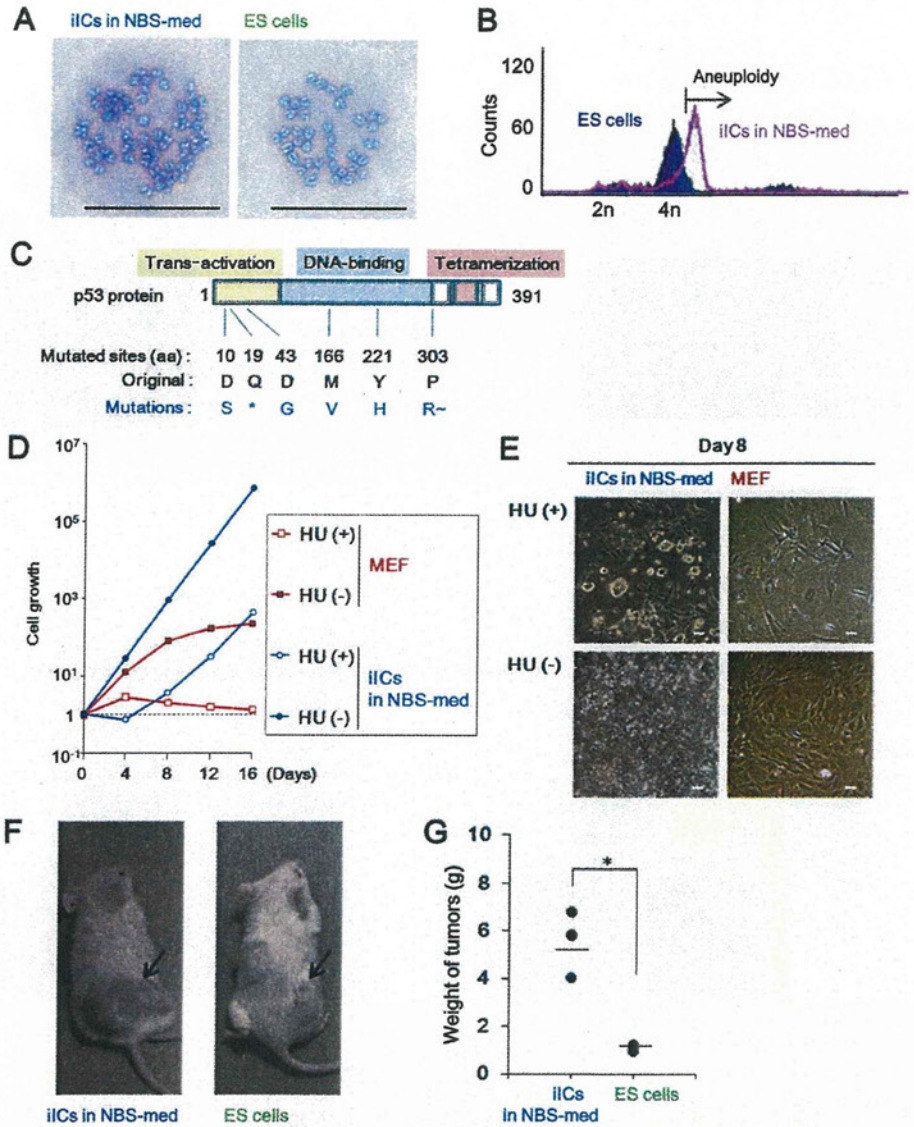

FIGURE 2. **iICs in NBS-med show cancerous characteristics.** *A* and *B*, aneuploidy is observed in iICs in NBS-med by Giemsa staining (*A*) and DNA content analysis (*B*) of M-phase cells. *C*, mutated p53 is frequently detected in iICs in NBS-med. The *asterisk* (*) indicates the stop codon. *R*~ indicates the resulting frameshift. *aa*, amino acids. *D* and *E*, the iICs in NBS-med show defective p53-dependent growth repression after treatment with low dose HU (0.2 mM). Growth curve (*D*) and morphology (*E*) are shown. *F* and *G*, enhanced tumorigenicity was observed in the iICs in NBS-med. *Arrows* indicate tumors (*F*) induced in NOD-SCID mice after transplantation. Tumor weights were measured 4 weeks after transplantation (*G*). *Scale bars*, 50 μm (*A* and *E*).

still maintained a largely undifferentiated status even under LIF withdrawal conditions. By contrast, the cGCs in FBS-med progressed through the steps of differentiation, lost *Klf4* expression, and acquired high expression of *Cdx2*, *Fgf5*, and *T* (Fig. 3*A*). Because *Klf4* expression is induced by LIF/Stat 3 signaling and implicated in ESC self-renewal (32), these results suggest that the acquisition of aberrant *Klf4* expression in iICs under NBS-med contributes to LIF-independent maintenance of an undifferentiated cell population. Furthermore, recent report showed that activated p53 promotes the differentiation of human ESCs by repressing the stem cell factors including Oct3/4 and Klf4 (33), implying that functional loss of p53-pathway also contributes the undifferentiated status in iICs in NBS-med.

FIGURE 1. **ESCs differentiating in NBS-med undergo senescence and subsequently aggregate in piled-up spheres.** *A*, an experimental design is shown. ESCs maintained with passaging every 2 days were held under three serum conditions. Cells were passaged as per ESC cultivation in each medium condition until passage 6 followed by continued maintenance with medium change. *B–D*, shown is piled-up sphere development via senescence. Representative images during differentiation induction in each condition are shown. After serial cell proliferation, cells in NBS-med senesced as indicated by the flattened and enlarged morphology (*B*; *arrows*) and β-galactosidase activity (*C*), which led to the development of piled-up colonies (representative image) (*D*). Cells in FBS-med did not show massive senescence (*B*; *arrows with dotted line*). ABS conditions did not induce subsequent proliferating cells (*B*, *P6 + 14 days*). *E* and *F*, piled-up sphere formation in each medium condition is shown. Although massive sphere development was observed in NBS-med, it was rarely observed in the other conditions. *G*, shown are normal MEFs senesced after serial proliferation, similar to the process seen during the differentiation of ESCs. *Scale bars*, 50 μm (*B–D* and *G*) or 2 cm (*E*).

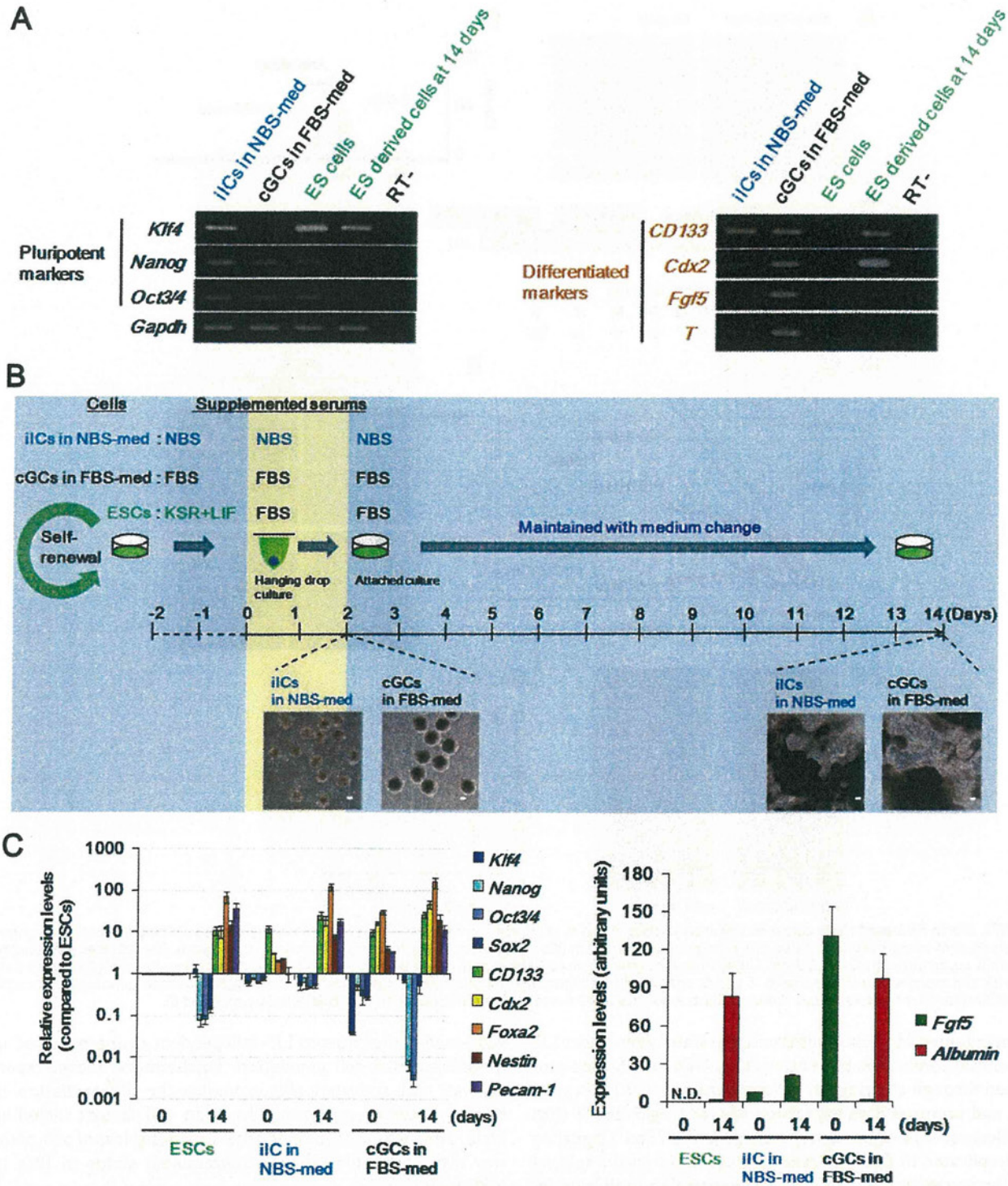

FIGURE 3. **iICs in NBS-med show stemness characteristics.** *A*, gene expression analysis is shown. Pluripotency and differentiation-associated gene expression status were compared in the indicated cells. ES derived cells at 14 days indicated the expression of each genes after differentiation for 14 days in a manner with Fig. 3*B*. *B*, experimental design is shown. Spontaneous differentiation was induced with EB formation by hanging-drop culture for 2 days and then seeded for attached culture. Inserted images are representative EBs (*left images*), and the resulting differentiated cells with multiple morphologies (*right images*) are indicated under each condition. *Scale bars*, 100 μm. *C*, gene expression analysis is shown. After differentiation induction, iICs in NBS-med still showed expression of pluripotency marker genes as well as differentiation marker genes in all germ layers.

To further investigate stem cell characteristics, we performed EB formation assays and examined self-renewal and differentiation capacities that are conserved in stem cells including CSCs (Fig. 3*B*). During adherent culture of the induced EBs from iICs in NBS-med and cGCs in FBS-med, cells in each condition were migrated, massively prolifer-

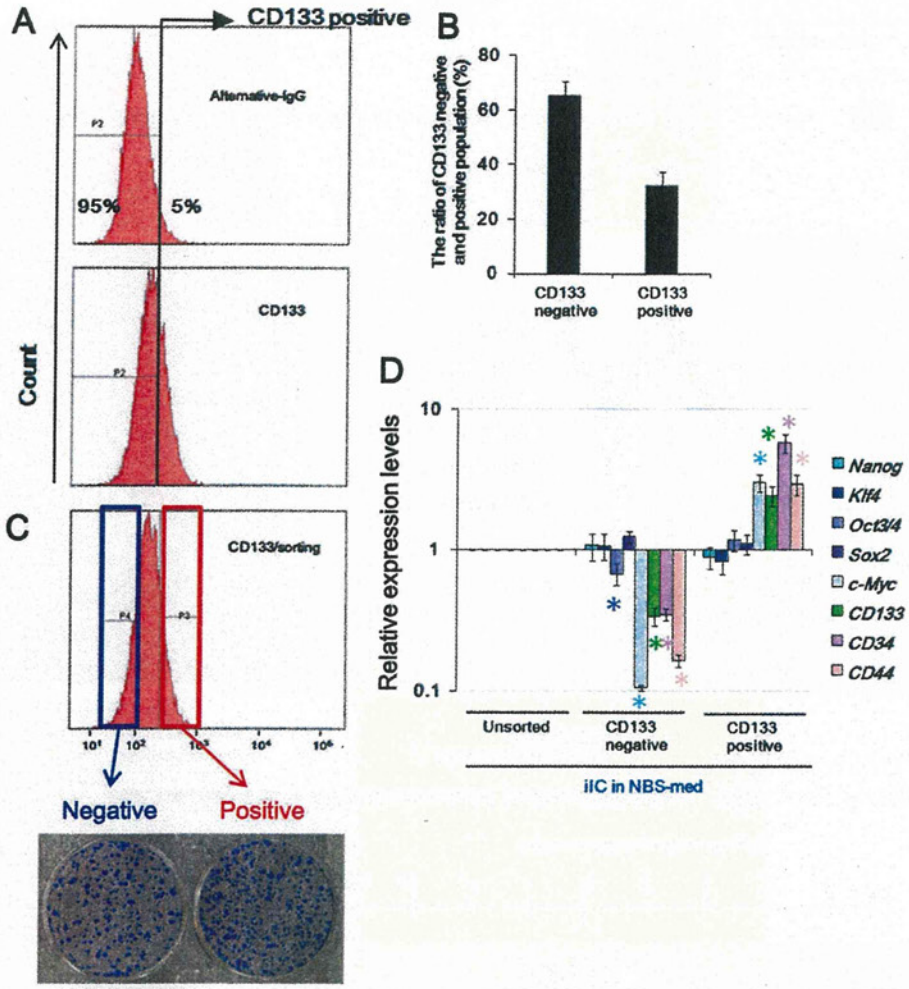

FIGURE 4. **CSC markers are enriched in CD133-positive fractions of iICs in NBS-med.** *A* and *B*, FACS analysis identified CD133-positive cells in iICs in NBS-med. The threshold discriminating CD133 positive/negative fractions was determined by negative control experiments using alternative IgG (*A*, *upper*). The CD133 positive-fraction was about 35% of iICs in NBS-med (*A*, *lower*, and *B*). *C*, both CD133-positive and -negative fractions developed spheres on methylcellulose. *D*, expression of ES-related and CSC-related marker genes was compared between CD133-positive and -negative fractions. Expression of *Oct3/4*, *c-Myc*, and CSC-related marker genes is significantly high in CD133-positive fraction.

ated, and developed into cells with different morphologies (Fig. 3*B*, *inserted images*), implying differentiation of the iICs in NBS-med and cGCs in FBS-med. Consistently, after adherent culture for an additional 11 days after EB formation (see the *images* in Fig. 3*B*), the resulting EB cells in each condition showed expression of differentiation marker genes in all three germ layers (Fig. 3*C*). Such three germ layer differentiation was also shown in the tumors that developed with the experiments as in Fig. 2 and (**supplemental Figs. S1 and S2**). Tumor formation assay *in vivo* also confirmed the pluripotency of these cells (**supplemental Fig. S2**). Intriguingly, although the expression of pluripotency markers was largely decreased in cultured EB derived from the cGCs in FBS-med or ESCs, the iICs in NBS-med still showed high expression of pluripotent marker genes even after the induction of differentiation. This indicates that the iICs in NBS-med retain several stemness characteristics even under differentiation conditions, a feature that may confer an advantage in tumor formation. Indeed, pluripotent marker genes are still highly expressed in tumors derived from iICs in NBS-med associated with enhanced tumor volume (**supplemental Fig. S2** and Fig. 2). Taken together our results indicate that the iICs in NBS-med are effectively cancerous stem cells that show both cancer cell characteristics and stemness properties.

CSC-related Markers Accumulated in the CD133-enriched Fraction of iICs in NBS-med—CSCs are identified by several markers in surface antigens, such as CD133 (34). To characterize the stem-like subpopulation in the iICs in NBS-med, as shown in Fig. 4*A*, the CD133-positive fraction that is about 35% of iICs in NBS-med (Fig. 4*B*) was separated from the CD133-negative fraction. Although sphere formation efficiency on methylcellulose (Fig. 4*C*) and the expression of *Nanog*, *Klf4*, and *Sox2* were shown without a major difference in both CD133-positive and -negative fractions, *Oct3/4* and *c-Myc* expressions were significantly lower in the CD133-negative fraction (Fig. 4, *A* and *B*). In addition, other CSC markers *CD34* and *CD44* was also highly expressed in the CD133 enriched cells (Fig. 4*D*). These results imply that, as a stem-like subpopulation, CD133-positive fractions could contribute to the maintenance of iICs

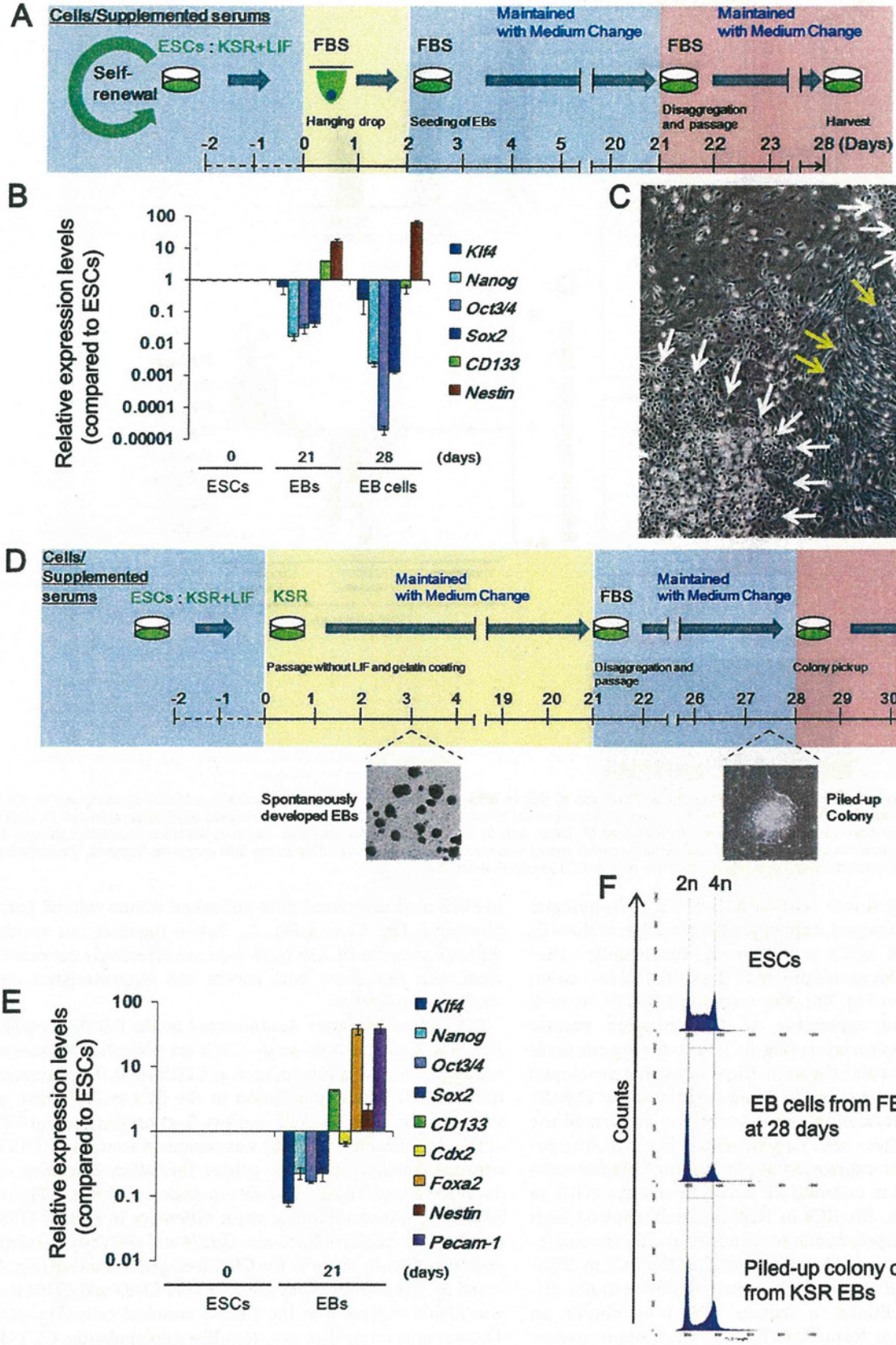

in NBS-med even under differentiation stress due to LIF independent expression of all Yamanaka factors (35). This identification poses another question in the status of cGCs in FBS-med.

cGCs in FBS-med Show Several Properties of Embryonal Carcinoma Cells—Similar to development of iICs under an aberrant serum environment, cGCs in FBS-med were also observed as a result of ESC cultivation under an aberrant serum environment compared with native development. As described above, the cGCs in FBS-med show neither the pile-up morphology nor major chromosomal instability and Arf-p53 module dysregulation (**supplemental Fig. S1, *A* and *B***), suggesting that cGCs in FBS-med are not malignant cancerous cells. However, they still expressed some pluripotent marker genes and showed differentiation capacities to three germ layers with slightly enhanced tumorigenicity compared with ESCs (**supplemental Fig. S1*D*** and Fig. 3). Intriguingly, the characteristics of cGCs in FBS-med are shared with embryonal carcinoma cells that are developed from primordial germ cells derailing from the migration track as well as transplanted early stage embryos; embryonal carcinoma cells are characterized with tumorigenicity, the abilities of LIF-independent multipotency, and differentiation to three germ layers (2, 36), analogous to stemness characteristics shown in cGCs (**supplemental Fig. S2** and Fig. 3). In addition, embryonal carcinoma cells are the pluripotent stem cells of teratocarcinoma with wild-type p53 and are quite responsive to chemotherapeutic drug treatment, which is also analogous to the features shown in cGCs (**supplemental Fig. S2**). Thus, a resulting population derived from the differentiated ESCs under an environmental aberrancy is analogous to that from the heterotopic transplantation of blastocysts and primordial germ cells.

Differentiation Environment in EBs Prevents Development of cGCs in FBS-med—Whereas ESCs as well as induced pluripotent stem cells possess the potential to enable regenerative medicine, this study poses the risk of development of CSCs and embryonal carcinoma cells under aberrant environments. This led us to investigate the CSC-like properties of ESC-derived cells that differentiated under several conditions *in vitro*. Expression of pluripotent marker genes were significantly reduced after differentiation by hanging drop culture in FBS-med at day 21 (Fig. 5, *A* and *B*). Such differentiated cells further underwent differentiation steps after disaggregating EBs and the additional adherent culture (Fig. 5*B*, *28 days*). Indeed, cells at 28 days massively differentiated in morphologically epithelial and fiber-like cells without detectable genomic instability (Fig. 5, *C* and *F*, *upper* and *middle*). Because non-serum conditions were also employed for ESC differentiation induction (37), genome stability was also tested under the conditions using KSR-med (Fig. 5*D*). ESCs in KSR/LIF(−) medium spontaneously led to EB-like structure formation and underwent differentiation (Fig. 5, *D* and *E*). Culture of dissolved EB cells led to some piled-up spheres in FBS-med (Fig. 5*D*); however, after cloning these spheres, most of them did not actively grow (22/24) (**supplemental Fig. S3*A***) or show epithelial-like morphology (1/24) (**supplemental Fig. S3*B***). Although a clone (1/24) could reform piled-up morphologies (**supplemental Fig. S3*C***), the ability to form a piled-up sphere in such cells was much weaker than that of iICs in NBS-med (**supplemental Fig. S3*C***) and did not accompany the chromosomal instability and Arf-p53 module dysregulation (Fig. 5*F*, *lower* and **supplemental Fig. S3*D***). Together these results suggest the importance of *in vitro* differentiation conditions to reduce the risk of developing unexpected populations.

Differentiating ESCs Accumulate DNA Damage and Activate Anti-cancer Barrier Responses—Although this study illustrated that ESCs can transform into cancerous stem cells during differentiation in NBS-med, a question remains regarding the mechanistic aspects of the inductions of genomic instability, mutations, and the resulting transformation. Growth curves of differentiating ESCs in aberrant conditions demonstrate initial proliferation but then eventual cessation of growth in all three culture conditions (Fig. 6*A*). Under these processes, it was observed that some fraction of the cells naturally undergo apoptosis at around P2-P3, as assessed by TUNEL staining (Fig. 6*B* and **supplemental Fig. S4*A***) and an increase of the sub-G_1 population by flow cytometry (Fig. 6*C* and **supplemental Fig. S4*B***). γH2AX that appeared to reflect DNA damage started to be detected at P1 by Western blotting before apoptosis induction and by immunostained foci observed at P2 (Fig. 6*D*, *a* and *b*); however, the increased γH2AX level was efficiently decreased in P3 cells in FBS- and ABS-med, coincident with a decrease in apoptotic events (Fig. 6, *C* and *Db*, and **supplemental Fig. S4, *C* and *D***). Together with the diminishment of H2AX in P3 cells (Fig. 6*Db*, compared with β-Actin signals) (38, 39), these results show that p53-dependent anti-cancer barrier reactions are activated in response to spontaneous DNA lesion formation, mirroring the initial stages of carcinogenesis.

ESCs Differentiating in NBS-med Undergo Senescence before the Development of Cancerous Stem Cells—Although carcinogenic stress and barrier responses were observed in differentiating ESCs under all three medium conditions, cancerous stem cells are only induced under NBS-med conditions. What exactly produces the difference in the differentiating ESCs? Unlike other conditions, damaged cells in NBS-med were not efficiently eliminated (Fig. 6*D*, *b* and *c*), thereby these cells with γH2AX but with diminished H2AX survived with a senescent morphology at P3-P5 (Fig. 1*B*, also see **supplemental Fig. S4*D***), under which pile-up spheres were eventually developed. Together with the accelerated genomic instability under H2AX haploinsufficiency by exogenous DNA lesions (40), our observations imply that senescent

FIGURE 5. **Differentiation environments affect the reduction of risks for cancerous stem cell development.** *A–C*, differentiation of ESCs via EBs is shown. The experimental scheme is shown (*A*). EB dissociation and the following culture further led to differentiation in accordance with the decreased expression of ES-related and neural stem cell-related genes and enhanced expression of a premature neuron marker gene (*Nestin*) (*B*). At 28 days, ES-derived cells showed epithelial-like (*white arrows*) and fiber (*yellow arrows*) morphology. *D* and *E*, differentiation of ESCs in KSR-med is shown. The experimental scheme is shown (*D*). ESCs were also differentiated to three germ layers in KSR-med (*E*). Dissolved EBs were seeded in FBS-med condition or KSR condition, although dissolved EBs seeded into KSR-med massively died (data not shown). *F*, DNA content analysis in each state of cells is shown. Differentiating ESCs under FBS-med or KSR-med did not develop major genome instability. *Scale bars*, 50 μm.

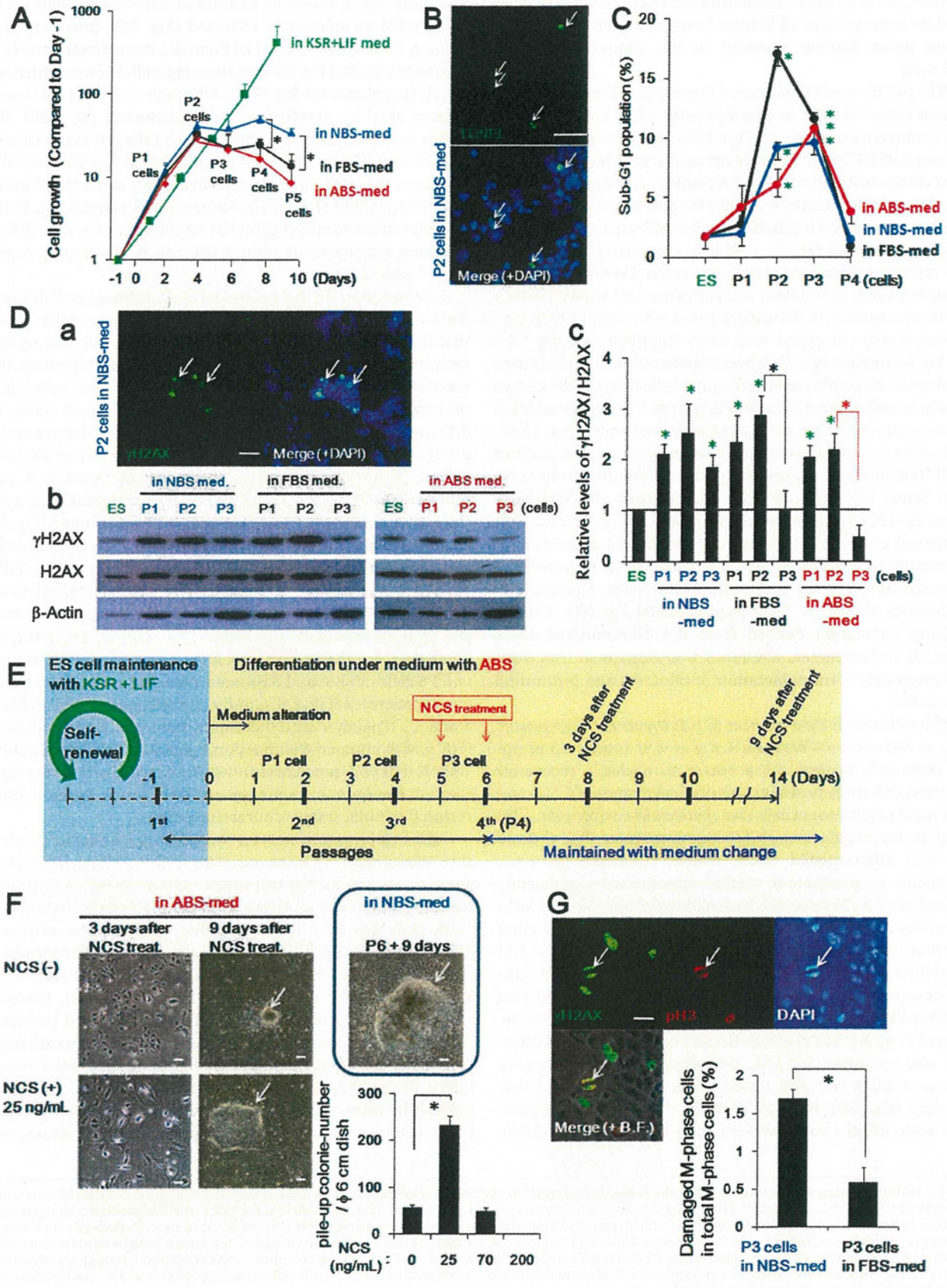

cells with irreparable DNA lesions undergo the carcinogenic transformation. To test this argument directly, we examined whether piled-up sphere formation was accelerated by the exogenous DNA lesions in the cells that have escaped the apoptotic event at P3. In ABS-med conditions, NCS treatment at 5 and 6 days promptly induced senescence-like morphology (Fig. 6, *E* and *F*, *3 days after NCS treatment*). At 9 days after NCS treatment, even in ABS-med conditions, NCS treatment induced piled-up sphere formation similar to the differentiating cells in NBS-med (Fig. 6*F*). Damage level was found to be critical to the frequency of pile-up sphere formation, which seemed to be optimum with 25 ng/ml NCS in this experiment (Fig. 6*F*). Thus, DNA lesions under down-regulated H2AX contribute to senescence induction in the differentiating ESCs and the resulting piled-up sphere formation.

Genomic instability development that is induced before MEF immortalization is ascribed to the carryover of irreparable DNA lesions to the M phase (8). In agreement with this, the irreparable DNA lesions in NBS-med were often carried over into the M phase of P3 cells before the development of iICs (Fig. 6*G*). Taken together, these results demonstrate that insufficient barrier reactions against carcinogenic stress permit the accumulation of aberrant DNA lesions in differentiating ESCs, leading into the development of induced cancerous stem cells.

A Condition with Lower FBS Concentration Leads to Accumulation of Senescent Cells under ESC Differentiation—The above results demonstrate that irreparable DNA lesions under diminished H2AX lead to senescence induction and resulting piled-up sphere formation during ESC differentiation. However, the question remains, Which factors in NBS-med conditions allow damaged cells to survive with senescence induction? To address this issue, we focused on the effect of growth acceleration that is produced by the different serum conditions and determined the effect of the exogenous growth acceleration by reducing the percentage of supplemented FBS (Fig. 7*A*) for the following reasons. 1) In the process of immortality development in MEFs, continuous growth acceleration by serum induces DNA double strand breaks due to DNA replication stress, which leads to the induction of senescence, genomic instability, and p53-module dysregulation, similar to the effect shown by oncogene acceleration (8, 38, 41, 42). 2) Temporary serum deprivation protects MEFs from immortality development under genome stability (38), suggesting that the level of growth acceleration could affect the balance between carcinogenic stress and an anti-cancer barrier. 3) During ESC differentiation we observed higher levels of subG$_1$ in FBS-med conditions compared with others (Fig. 6, *A* and *C*, *P2*), potentially suggesting that the difference in the enriched growth factors in FBS gives the difference in the stress-barrier balance. ESCs differentiated under 20, 10, and 5% FBS-med conditions initially proliferated in proportion to the serum concentration (Fig. 7*B*, *3 days*) and eventually stopped the growth (*6–9 days*). These differentiating cells exhibited γH2AX signaling (Fig. 7*C*, *3* and *6 days*) followed by H2AX diminishment (*9 days*). When γH2AX was presented, these cells were also subjected to apoptosis induction as shown by PARP1 cleavage (3 and 6 days) in all conditions, suggesting the activation of carcinogenic stress and the barrier responses. However, only in 10% FBS-med conditions, senescent cells are massively developed at 9 days, which was unexpectedly not shown either in higher or in lower serum conditions but only in the intermediate (Fig. 7*D*). These results illustrated that, for differentiating stem cells, a potential pitfall leading to senescence induction was generated between growth stimulation levels in the surrounding environment, probably associated with the balance between the barrier responses and cell maintenance.

Sufficient Barrier Reactions Prevent Senescence Induction in Differentiating ESCs—To prevent cancer stem cell development, the above results suggest that sufficient barrier activation protects the damaged cells from senescence and the resulting transformation. To confirm this issue, we treated P1 and P2 cells in NBS-med with Akt inhibitor IV and PARP inhibitor AZD2281 (Fig. 8*Aa*) because Akt is a major target of several anti-cancer drugs, such as sorafenib (43, 44) and PARP inhibitors also act as an anti-cancer drug (45). As expected, treatment of Akt inhibitor IV or AZD2281 significantly reduced the surviving cells during differentiation of ESCs in NBS-med (Fig. 8*Ab* and **supplemental Fig. S5**), associating with the protection from the accumulation of senescent cells (Fig. 8*Ac*). Because an effect of PARP inhibition is partial DNA repair deficiency, the effect of spontaneous DNA damage was further tested by withdrawal of monothioglycerol that reduces reactive oxygen species that lead to stress and contributes to the reduction of DNA damage (46–48). Again, culture conditions without monothioglycerol led neither to survival with a senescent state nor to the development of piled-up spheres (Fig. 8B). This supports that sufficient barrier activation prevents cancerous stem cell development, in which appropriate treatment with an anti-cancer drug might help. However, such an argument might be carefully treated because the effects of DNA damage could lead to different outputs which depend on cellular conditions (Fig. 6, *E* and *F*).

FIGURE 6. **Carcinogenic stress is induced during differentiation of ESCs in aberrant environments.** *A*, cell growth in each medium condition is shown. Unlike continuously growing ESCs in the KSR + LIF condition, differentiating cells under each condition were growth-arrested at P2-P3. *B* and *C*, massive apoptosis induction was observed at P2-P3 with the TUNEL assay (*B*) and sub-G$_1$ fractions (*C*). *ES*, embryonic stem. Sub-G$_1$ fraction analysis revealed that apoptosis is mainly induced at P2-P3, which coincides with growth suppression (*A*). *D*, the status of spontaneously accumulated DNA lesions was determined by γH2AX foci formation (*Da*, also demonstrated in **supplemental Fig. S3C**) as well as γH2AX signal detection with Western blotting (*Db*). γH2AX signals were diminished at P3 in the differentiating cells in FBS- and ABS-med but not significantly decreased in cells in NBS-med (see *P2* and *P3* and quantified Fig. 4*Dc*). *E* and *F*, additional DNA damage accelerates the piled-up sphere formation. Experimental design is shown in *E*. ESCs were maintained and differentiated in ABS-med as in Fig. 1*A*, but the P3 cells in P3 + 1 day were treated with NCS for 3 days. After NCS treatment, cells were maintained with medium change as cells rapidly senesced (*F*, *3 days after NCS treatment*). NCS treatment allows differentiating ESCs to form spheres in ABS-med. Images are representative, showing senescent cells, and resulting sphere development was induced under ABS-med with 25 ng/ml NCS treatment (*F*). The frequency of piled-up sphere development in ABS-med was also determined with different NCS doses (*F*, *graph*). Different than the Fig. 1 results, we observed piled-up colony formation in non-NCS-treated conditions, implying that a decrease in the times of passage allowed remaining undifferentiated cell proliferation. *Scale bars*, 100 μm. *G*, the status of DNA lesions in M-phase cells was determined by co-localized staining of γH2AX and phosphorylated histone H3 (pH3) (*arrows*). Images are representative. The quantified results are also shown (graph), indicating DNA-lesion carryover into the M phase. *Scale bars*, 50 μm.

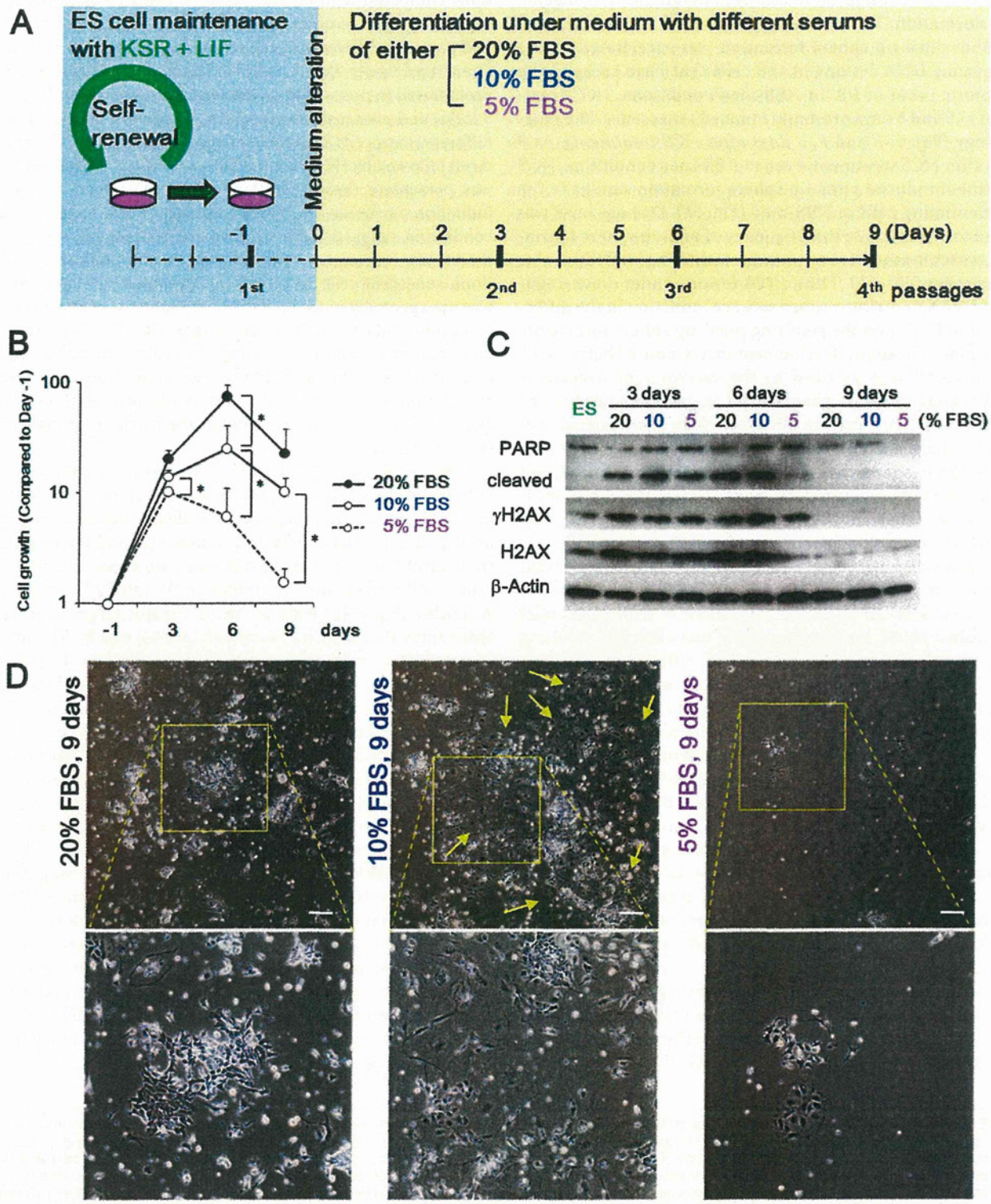

FIGURE 7. **Decreased intensity of growth acceleration could induce senescence-like morphology of differentiating ESCs in FBS-med.** *A*, experimental design is shown. ESCs maintained with passaging every 2 days were held under 20, 10. Cells were passaged every 3 days in each medium condition until 9 days. *B*, shown is the growth curve of differentiating ESCs in the indicated conditions. A high concentration of FBS induced strong cell proliferation. *C*, DNA damage response in differentiating ESCs is shown. Western blotting shows PARP1 cleavage (3 and 6 days), γH2AX up-regulation (3 and 6 days), and H2AX diminishment (9 days) in differentiating ESCs. ES, *ES*, embryonic stem. *D*, cell morphologies in each medium at 9 days is shown. Senescence was not observed in 20 and 5% FBS condition, but differentiating ESCs in 10% FBS condition showed flattened and enlarged morphology. *Lower panels* show expanded images of the squares in the *upper panels*. *Yellow arrows* indicate the representative cells showing flattened and enlarged morphology. *Scale bars*, 50 μm.